

Deep Learning Waveform Channel Modeling for Wideband Optical Fiber Transmission: Model Comparisons, Challenges and Potential Solutions

Minghui Shi, Hang Yang, Zekun Niu, Chuyan Zeng, Yunfan Zhang, Junzhe Xiao, Mingzhe Chen, Weisheng Hu, and Lilin Yi

Abstract—Fast and accurate waveform simulation is critical for understanding fiber channel characteristics, developing digital signal processing(DSP) technologies, optimizing optical network configurations, and advancing the optical fiber transmission system towards wideband. Deep learning (DL) has emerged as a powerful tool for waveform modeling, offering high accuracy and low complexity compared to traditional split-step Fourier method (SSFM), due to its strong nonlinear fitting capabilities and efficient parallel computation. However, most DL methods are designed for few-channel and low-rate wavelength division multiplexing (WDM) systems, leaving their scalability to wideband systems uncertain. Moreover, the lack of a standardized accuracy evaluation method and the inconsistent results between waveform errors and transmission performance errors, hinders fair comparisons and comprehensive analyses of various DL schemes. In this paper, we introduce a DSP-assisted accuracy evaluation method integrated with nonlinear DSP, providing a fair benchmark for evaluating the accuracy of DL models. Using this method, we conduct a comprehensive comparison of DL schemes, ranging from simple few-channel and low-rate configurations to more complex wideband setups. The feature decoupled distributed method combining with bidirectional long short-term memory (FDD-BiLSTM) achieves the better performance compared to other DL schemes in 5-channel and 50 Gbaud configurations. Furthermore, in scenarios with more-channel and higher-rate, the performance advantages of FDD-BiLSTM will be further improved. These advantages are attributed to the combining of distributed method, physical prior knowledge and temporal neural network. However, as the number of channels and symbol rates increase, the performance of FDD-BiLSTM still gradually deteriorate. We analyze these challenges from three perspectives: the more intricate linear and nonlinear effects, the higher sampling rate required for SSFM. To address these challenges, we discuss potential solutions from two aspects: incorporating more prior physical knowledge and optimizing the structure of DL models. We believe that with the continuous progress in technology, these challenges in wideband systems will be gradually overcome, positioning DL schemes as a promising waveform modeling technology to drive the development of next-generation optical networks.

Index Terms—Deep learning (DL), optical fiber channel mod-

This paragraph of the first footnote will contain the date on which you submitted your paper for review, which is populated by IEEE. This work was supported by the National Key R&D Program of China (2023YFB2905400), National Natural Science Foundation of China (62025503), and Shanghai Jiao Tong University 2030 Initiative. (Minghui Shi and Hang Yang contributed equally to this work). (Corresponding author: Lilin Yi and Zekun Niu)

The authors are with the State Key Laboratory of Photonics and Communications, School of Electronic Information and Electrical Engineering, Shanghai Jiao Tong University, Shanghai 200240, China (email: minghuishi@sjtu.edu.cn; hangyang@sjtu.edu.cn; zekunniu@sjtu.edu.cn; z-mary@sjtu.edu.cn; yunfanzhang@sjtu.edu.cn; xiaojunzhe@sjtu.edu.cn; cmz1461404680@sjtu.edu.cn; wshu@sjtu.edu.cn; lilinyi@sjtu.edu.cn).

eling, waveform-level simulation, wideband wavelength division multiplexing (WDM) system.

I. INTRODUCTION

THE growing demand for data traffic is driving the evolution of optical fiber communication towards wideband, high-rate, and large-capacity systems, expanding the spectral coverage beyond the traditional C-band [1]–[5]. Accurate, reliable, and fast optical fiber transmission simulation systems are crucial for optimizing optical networks [6]–[11], advancing digital signal processing (DSP) algorithms [12]–[17], and enabling end-to-end (E2E) optimization [18]–[24]. Fiber channel modeling plays a pivotal role in these simulation systems, providing critical insights into the signal evolution process within optical fibers. The propagation of signals through optical fibers is governed by the nonlinear Schrödinger equation (NLSE) [25]. Except for a few special cases, the NLSE lacks an analytical solution and must be solved through numerical simulation.

Gaussian noise (GN) [26] and enhanced Gaussian noise (EGN) models [27] offer accurate and fast fiber channel modeling techniques, primarily focusing on power-level simulations. These models treat fiber nonlinearities as Gaussian noise and estimate the generalized signal-to-noise ratio (GSNR). However, GN-like models fail to provide detailed signal waveform information, limiting their applicability in DSP algorithm design and optimization, such as nonlinearity compensation. The split-step Fourier method (SSFM) [28] is a waveform-level modeling technique for optical fiber channels. It divides the entire optical fiber link into multiple small segments, addressing linear and nonlinear effects separately within each segment. However, SSFM requires numerous iterations, leading to high computational complexity that typically scales with the fourth power of bandwidth [29]. For wideband, long-haul systems, this computational inefficiency becomes especially pronounced, resulting in simulation times of several hours for a single parameter. Therefore, an efficient waveform-level channel modeling tool is critical to support the evolving demands of wideband optical communication systems.

Recently, deep learning (DL) techniques have gained significant attention for optical fiber channel waveform modeling, offering a promising balance between accuracy and complexity. This is attributed to their superior nonlinear fitting capabilities [30] and efficiency in parallel computation [31].

A bidirectional long short-term memory (BiLSTM) [32] has been proposed to model 10 to 80 km optical fiber channel in intensity modulation and direct detection (IMDD) systems. A conditional generative adversarial network (CGAN) [33] has been proposed in a coherent systems with 1000 km transmission. The multi-head attention mechanism [34], [35], Fourier neural operators (FNO) [36] and center-oriented LSTM (CoLSTM) [37] have been proposed to model long-haul transmission in a distributed manner by cascading multiple DL models in single-channel systems. A physics-informed neural operator (PINO) [38] has been introduced to reduce the requirements of training dataset by integrating physical principles. A fully connected neural network (FCNN) [39] and FNO [40] have been introduced to achieve accurate channel modeling in few-channel WDM systems. A BiLSTM-based feature decoupled distributed (FDD-BiLSTM) scheme [41], [42] combining DL models and physical models to handle linear and nonlinear effects respectively, has been extended to multi-channel WDM systems. The deep operator network (DeepONet) [43] scheme has been applied to wideband WDM configurations covering the C+L band, although it neglects inter-channel nonlinear effects. [44]–[46] have investigated the influence of different system parameters on the accuracy and generalization ability of DL models. Beyond optical fiber transmission systems, DL technologies have also been applied to other systems, such as multi-core and few-mode optical fiber link [47], [48], radio over fiber (RoF) link [49], orthogonal frequency division multiplex (OFDM) systems [50], free space optical communications (FSO) [51] and nonlinear photonics [52]–[62].

DL methods present a viable alternative to traditional waveform-level channel modeling techniques. However, these approaches are typically designed for few-channel, low-rate or simplified wideband scenarios, where the number of WDM channels is fewer than 5, and the transmission rate is below 100 GBaud. Although they have potential to extend to wideband systems, a fair performance comparison and comprehensive analysis in the multi-channel and high-rate cases are still lacking. Furthermore, a standardized accuracy evaluation method is essential for a fair comparison. Currently, the accuracy evaluation of DL models often employs normalized mean square error (NMSE) with a threshold of 0.02 as a benchmark for waveform errors assessment [32]. Additional metrics, such as GSNR and Q-factor, are also used to evaluate transmission performance. However, the consistency between waveform errors and transmission performance errors remains unclear, and the NMSE threshold of 0.02 may not be universally sufficient, particularly in more complex wideband systems. Therefore, further investigation into the development of a fair and standardized accuracy evaluation method is necessary.

In this paper, we introduce a DSP-assisted accuracy evaluation method that combines both waveform and transmission performance to provide a fair and comprehensive evaluation of DL models. This method leverages both linear and nonlinear DSP algorithms to assess the impact of various types of impairments in the signal modeled by DL models, ensuring consistency between waveform errors and transmission performance errors. Using this DSP-assisted accuracy evaluation method,

we design scenarios of increasing complexity to thoroughly compare the performance of various DL schemes, including overall and distributed schemes, pure data-driven and data-physic hybrid-driven schemes, as well as neural networks and neural operators. In a 5-channel, 50 GBaud scenario, distributed schemes outperform overall schemes. Among more advantageous distributed schemes, temporal neural networks, such as BiLSTM, multi-head attention, and FDD-BiLSTM, surpass fully connected networks like FNO and DeepONet, demonstrating an 83.1% improvement in NMSE and a 1.06 dB reduction in Q-factor error. The comprehensive comparison reveals that FDD-BiLSTM and BiLSTM are the best schemes for simpler scenarios. Therefore, we extend the testing scenarios to more-channel and higher-rate configurations, including a 13-channel, 50 GBaud setup and a 5-channel, 100 GBaud setup. In both cases, the data-physic hybrid-driven scheme, FDD-BiLSTM, outperforms the pure data-driven BiLSTM. Further tests on FDD-BiLSTM across varying channel numbers and symbol rates in wideband configurations reveal significant performance degradation: NMSE increases by 92.9%, and Q-factor errors rise by 2.02 dB when scaling from 5 to 25 channels; similarly, NMSE degrades by 89.7%, and Q-factor errors increase by 1.33 dB when symbol rates increase from 50 to 200 GBaud. We analyze the challenges associated with scaling DL models to wideband configurations, including the more intricate linear and nonlinear effects, as well as the higher sampling rates. Finally, to enhance the application of DL schemes in wideband systems, we discuss potential solutions, including incorporating more prior physical knowledge and optimizing the structure of DL models.

The rest of the paper is organized as follows. Section II describes the SSFM-based optical fiber transmission simulation systems. Section III details the architecture of DL schemes and their training processing. Section IV discusses the limitations of current accuracy metrics and introduces the DSP-assisted accuracy evaluation method. Section V presents a comprehensive comparison of DL models across scenarios of increasing complexity using the DSP-assisted accuracy evaluation method, along with a discussion of the challenges in applying DL models to wideband configurations. Section VI discusses potential solutions to improve the accuracy of DL models in wideband systems. Finally, Section VI concludes the paper.

II. SSFM-BASED OPTICAL FIBER TRANSMISSION SIMULATION SYSTEM

This part introduces the structure of the SSFM-based optical fiber transmission simulation system, which generates the dataset for subsequent DL model training and serves as a baseline for accuracy evaluation.

The typical SSFM-based optical fiber transmission simulation system is shown in Fig. 1, including the transmitter, optical fiber channel, and receiver. At the transmitter side, bit sequences are generated using a pseudo-random number seed and mapped to symbol sequences via dual-polarized 16 quadrature amplitude modulation (DP-16QAM). The symbol sequences are then upsampled by a factor of 4. A root-raised cosine (RRC) filter is applied for pulse shaping, with a roll-off

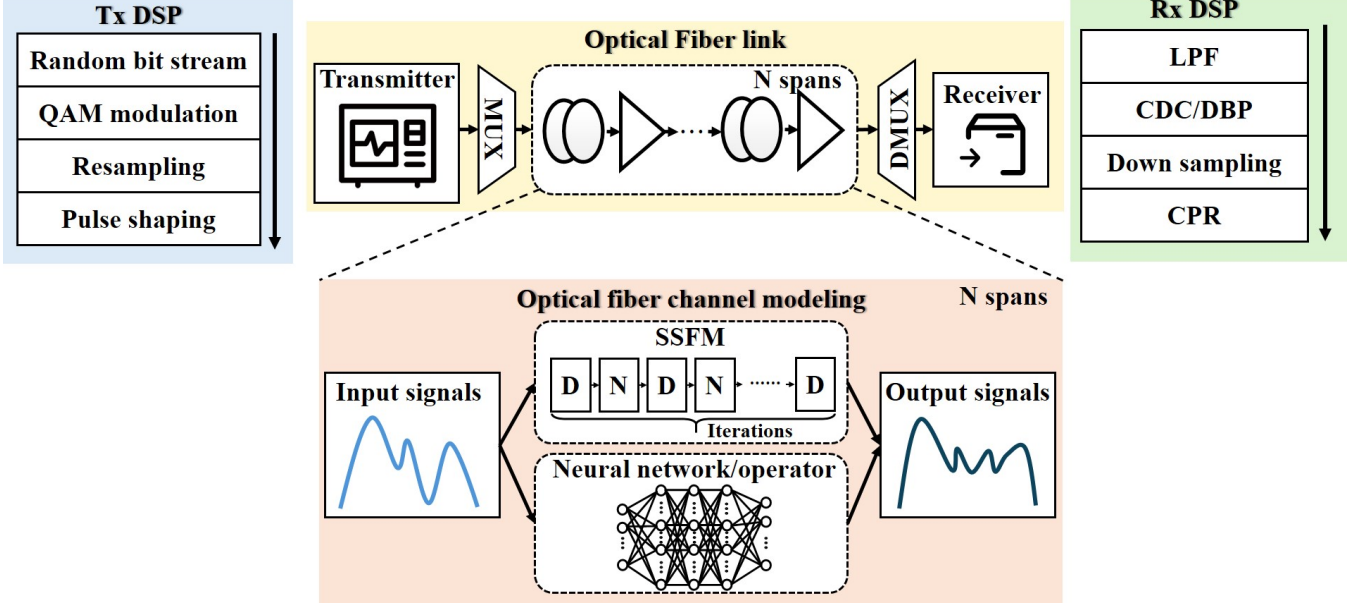


Fig. 1. The structure of a coherent optical transmission simulation system.

TABLE I
PARAMETERS OF SIMULATION SYSTEM

Parameters	Value
Modulation format	DP-16QAM
Roll-off factor of RRC	0.1
Carrier wavelength	1550 nm
Attenuation	0.2 dB/km
Dispersion	17 ps/(nm· km)
Nonlinear coefficient	1.3/(W· km)
Span length	80 km
EDFA noise figure	5 dB
Maximum nonlinear phase rotation of SSFM	0.005

factor of 0.1. Subsequently, the signals from different channels are modulated onto separate frequency carriers to create full-field WDM signals for transmission within the optical fiber channel. The WDM signals can be expressed as follows:

$$\mathbf{A}(z, t) = \sum_{k=1}^C \mathbf{A}_k(z, t) \exp(j\Delta\omega_k t), \quad (1)$$

where \mathbf{A} represents the optical signals over two arbitrary orthogonal polarization modes \mathbf{A}_x and \mathbf{A}_y . \mathbf{A}_k is the optical signal of k -th channel. z indicates the transmission distance and t represents the time coordinate. C is the total number of WDM channels, and $\Delta\omega_k = \omega_k - \omega_0$ is the difference between the central frequency of k -th channel and the central frequency of WDM signals.

The propagation of optical signal through the single-mode fiber (SMF) is governed by the NLSE [28], which is expressed as:

$$\frac{\partial \mathbf{A}(z, t)}{\partial z} = (\hat{\mathbf{D}} + \hat{\mathbf{N}})\mathbf{A}, \quad (2)$$

where \mathbf{D} is the linear operator that accounts for the effects of attenuation and chromatic dispersion (CD), and \mathbf{N} is the nonlinear operator that represents the effects of self-phase modulation (SPM), cross-phase modulation (XPM), and four-wave mixing (FWM) related to the signal energy. When dealing with dual-polarization signals, the NLSE is typically considered in its coupled form, known as the Coupled NLSE (CNLSE) [63], or CNLSE simplified version, the Manakov equation [64], [65]. Here, we employ the Manakov equation to model the fiber channel, which can be expressed as:

$$i \frac{\partial \mathbf{A}}{\partial z} - \frac{1}{2} \beta_2 \frac{\partial^2 \mathbf{A}}{\partial t^2} + \frac{8}{9} \gamma |\mathbf{A}|^2 \mathbf{A} + \frac{\alpha}{2} i \mathbf{A} = 0, \quad (3)$$

where β_2 is the group velocity dispersion parameter, γ is the nonlinear parameter and α is the loss parameter.

The SSFM is the most commonly used numerical method for solving the NLSE. The SSFM divides long-haul optical fiber into numerous small steps, allowing linear and nonlinear operators to be considered independently. The symmetric SSFM operation [66] at each step is expressed as:

$$\begin{aligned} \mathbf{A}(z + h, t) \approx & \exp\left(\frac{h}{2} \hat{\mathbf{D}}\right) \exp\left\{h \hat{\mathbf{N}} \left[\mathbf{A}\left(z + \frac{h}{2}, t\right)\right]\right\} \\ & \times \exp\left(\frac{h}{2} \hat{\mathbf{D}}\right), \end{aligned} \quad (4)$$

where h is the length in each step. The nonlinear phase rotation method [67], a variable step-size method, is employed, designed for systems dominated by nonlinearity. The sampling rate in SSFM is 4 times the channel number. According to their characteristics and computational convenience, the linear and nonlinear operators are calculated in the frequency and time domains, respectively. At the end of each fiber span, Erbium-doped fiber amplifiers (EDFA) are used to compensate for signal attenuation and introduce amplified spontaneous emission (ASE) noise, which can be approximated as Gaussian

TABLE II
DL-BASE WAVEFORM-LEVEL CHANNEL MODELING SCHEMES IN OPTICAL FIBER TRANSMISSION SYSTEMS

Schemes	Transmission mode	Driving mode	Network structure	Channel number	Symbol rate (GBaud)	Modulation format	Distance (km)	Reference
BiLSTM	△	□	◊	1	10	PAM4	80	[32]
CGAN	△	□	◊	1	30	16QAM	1000	[33]
Multi-head Attention	▲	□	◊	1	40	16QAM	1000	[34], [35]
FNO	▲	□	◆	1	28	64QAM	1200	[36]
Co-LSTM	▲	□	◊	1	32	DP-16QAM	2800	[37]
PINO	▲	■	◆	1	14	16QAM	320	[38]
FCNN	▲	□	◊	2	30	16QAM	80	[39]
FNO	▲	□	◆	5	30	DP-16QAM	800	[40]
FDD-BiLSTM	▲	■	◊	41	30	DP-128QAM	1040	[41], [42]
DeepONet	▲	□	◆	96	100	DP-16QAM	800	[43]

¹ Overall: △ Distributed: ▲ Pure data-driven: □ Data-physic hybrid-driven: ■ Neural network: ◊ Neural operator: ◆

noise. The parameters of simulation systems utilized in this paper are summarized in Table 1.

After transmission through the optical fiber channel, demultiplexing is performed to extract the signal in the channel under test (CUT). Receiver-side DSP (Rx DSP) is then employed to compensate for signal impairments. A matched RRC filter is first applied, followed by down-sampling. Chromatic dispersion compensation (CDC) is then performed to address linear impairments. Alternatively, the CDC can be replaced by the digital backpropagation (DBP) algorithm [68], which compensates for both linear and nonlinear impairments, providing a more thorough analysis of the nonlinear modeling capacity of DL models. Next, carrier phase recovery (CPR) and demodulation are executed. Finally, the GSNR and Q-factor are calculated to evaluate the transmission performance.

The waveforms of full-field WDM signals generated from the SSFM-based simulation system provide a rich dataset for training DL models. During testing, the same Tx and Rx process and parameters are employed to evaluate performance differences between SSFM-based and DL-based optical fiber channels.

III. DL OPTICAL FIBER CHANNEL WAVEFORM MODELING

The primary computational burden in optical fiber transmission simulation arises from the SSFM. As a result, the DL schemes primarily focus on modeling the optical fiber channel. In the following, we outline the classification of DL-based optical fiber channel modeling schemes and introduce the dataset construction and training process for the DL models.

A. Classification of DL schemes

DL schemes utilize parameterized neural networks or operators to uncover hidden correlations and patterns from datasets generated by SSFM-based simulations, eliminating the need for complex prior mathematical and physical knowledge. Advanced DL schemes have achieved efficient optical fiber channel waveform modeling. In this section, we provide a comprehensive review of DL schemes. To offer a clear and

detailed introduction and comparison of various DL schemes, we have categorized them into three classes based on their distinct characteristics, including transmission modes, driving modes, and network architectures.

- Transmission mode refers to whether a single model or multiple models are used to model long-distance optical fiber link transmission. This can be divided into overall and distributed schemes.
- Driving mode refers to whether physical knowledge is integrated alongside data-driven approaches. This can be classified into pure data-driven or physics-data hybrid-driven schemes.
- Network structure refers to the differences between various parameterized architectures, which can be divided into neural networks and neural operators.

1) **Overall schemes and distributed schemes:** Optical fiber links typically consist of several components: optical fibers, optical amplifiers, and other optical devices. Long-haul optical transmission links are composed of a cascade of multiple optical fibers and optical amplifiers. To model long-haul optical links, DL schemes typically utilize two main approaches: overall schemes and distributed schemes, which use a single or multiple DL models to achieve long-haul transmission.

Overall schemes treat the fiber link as a single integrated module and use a single network to model the entire fiber link. Examples of this approach include the overall BiLSTM [32] and the overall CGAN [33]. The overall BiLSTM scheme is the first DL optical fiber channel modeling scheme and has demonstrated high accuracy in intensity modulation and direct detection (IMDD) systems over distances ranging from 10 to 80 km. However, it is limited to short-distance transmission due to the deterministic nature of BiLSTM, which struggles to effectively fit random noise introduced by EDFA between fiber spans. To extend the capacity of DL models to long-haul transmissions, the CGAN scheme was introduced. As a generative model, CGAN can fit specific distributions to address the challenge of fitting random noise. It has achieved fast and accurate fiber channel modeling, up to 1000 km,

in coherent transmission systems. However, the adversarial training approach of CGAN can be difficult to converge to optimal performance [69], [70], which particularly limits its application in multi-channel WDM systems.

Distributed schemes were developed to enhance the capabilities of DL schemes by mimicking the actual cascaded structure of long-haul optical fiber links. In distributed schemes, the entire optical fiber link is treated as multiple modules rather than a single integrated module, with each DL model responsible for modeling one fiber span. This allows for more flexible handling of random noise between spans. Related studies utilizing this structure include multi-head attention mechanism, FNO, Co-LSTM, PINO, FCNN, FDD-BiLSTM, and DeepONet. In these works, each model employs the same or slightly fine-tuned parameters to model the response of a single fiber span, with multiple models cascaded to achieve long-haul transmission. Distributed schemes have demonstrated robust performance in both single- and multi-channel WDM systems. By focusing on the characteristics of a single fiber span, these schemes avoid the complexities associated with modeling the entire fiber link, such as the accumulation of linear and nonlinear effects over distance and the amplifier noise, which is challenging for deterministic DL models. This simplification of features enables faster convergence and improved accuracy in DL models. Additionally, distributed schemes allow for flexible adjustments in transmission length by varying the number of cascaded models. However, the iterative cascading of multiple models introduces inevitable iterative errors, which can degrade performance in long-haul transmission. Some studies address these iterative errors by constructing multi-span datasets for training DL models [42] or by fine-tuning the models used in later spans [37], [38]. Despite challenges posed by iterative errors, distributed schemes offer higher accuracy and flexibility compared to overall schemes. As such, they are seen as potential mainstream methods for fiber channel modeling in wideband and long-haul optical transmission systems.

2) Pure data-driven schemes and data-physics hybrid-driven scheme: DL schemes directly learn the mapping relationship between input and output signals collected from SSFM-based simulations and do not require extensive prior physical knowledge, which characterize them as pure data-driven schemes. To improve accuracy, some studies incorporate prior physical knowledge, resulting in data-physics hybrid-driven schemes.

Pure data-driven schemes rely solely on data collected from the SSFM-based simulations, including pairs of channel input and output waveforms. During training, loss functions such as mean squared error (MSE) or smooth L1 (SL1) loss are used to optimize the model, allowing it to converge to the features present in the training data. These schemes are valued for their simplicity in structure and training. However, they face the challenge of requiring the model to learn all characteristics of the data, including complex linear, nonlinear, and random effects within the optical fiber channel. Furthermore, pure data-driven models rely solely on waveform errors as loss functions, which may lead to suboptimal solutions that fail to satisfy the properties of the NLSE.

To enhance the accuracy of pure data-driven methods, data-physics hybrid-driven schemes have been proposed to integrate physical principles into the data preprocessing or training process. Representative examples of these approaches are FDD and PINO. The FDD scheme separates optical channel characteristics into linear and nonlinear components, with physical models employed for modeling linearity, while neural networks model nonlinearity. FDD ensures highly accurate linear modeling while reducing the complexity of neural network fitting features and improving the accuracy of nonlinear modeling. The PINO scheme integrates physical principles into the training process by utilizing DeepONet for channel modeling, with the NLSE embedded in the loss function. This allows for unsupervised training, significantly reducing the amount of training data required and improving training efficiency. Compared to pure data-driven methods, both PINO and FDD have demonstrated higher accuracy in both single-channel and multi-channel WDM systems. Additionally, hybrid models help circumvent the issues of suboptimal solutions and failure to satisfy NLSE properties commonly encountered in pure data-driven models.

3) Neural network schemes and neural operator schemes: DL schemes relying on neural networks have exhibited outstanding results in optical fiber channel modeling. In recent years, the development of deep neural operators as a novel DL approach has progressed rapidly, demonstrating strong generalization capabilities as solvers of partial differential equations (PDEs) [71]–[73].

Neural networks, supported by the universal approximation theorem, can approximate any continuous function with arbitrary precision, given sufficient depth and complexity. Neural networks learn mappings between discrete vector spaces. Various neural networks, such as CGAN, BiLSTM, and Transformer, have demonstrated high accuracy in optical fiber channel modeling. CGAN consists of two parts: the generator and discriminator. Through adversarial training, the generator mimics data distributions to fool the discriminator. However, CGAN faces challenges with convergence in complex multi-channel WDM systems. BiLSTM, a typical variant of recurrent neural networks (RNNs), captures temporal correlations through its forward and backward recurrent structures. Transformer leverages a self-attention mechanism, offering parallel computation capabilities and overcoming the long-term memory issues typical of RNNs. These models have been successfully applied in both single-channel IMDD systems and WDM coherent systems.

Neural operators represent a paradigm shift by learning mappings between infinite-dimensional function spaces, a more generalized approach compared to discrete vector spaces typically handled by neural networks. Two typical neural operators, FNO and DeepONet, have been introduced in optical fiber channel modeling. FNO utilizes Fourier transform techniques to create new solution maps for the NLSE from both time-domain and frequency-domain perspectives in single-channel and multi-channel WDM systems. DeepONet, consisting of branch and trunk networks, excels at capturing the intricate relationships between input and output functions. This operator can incorporate the NLSE into its

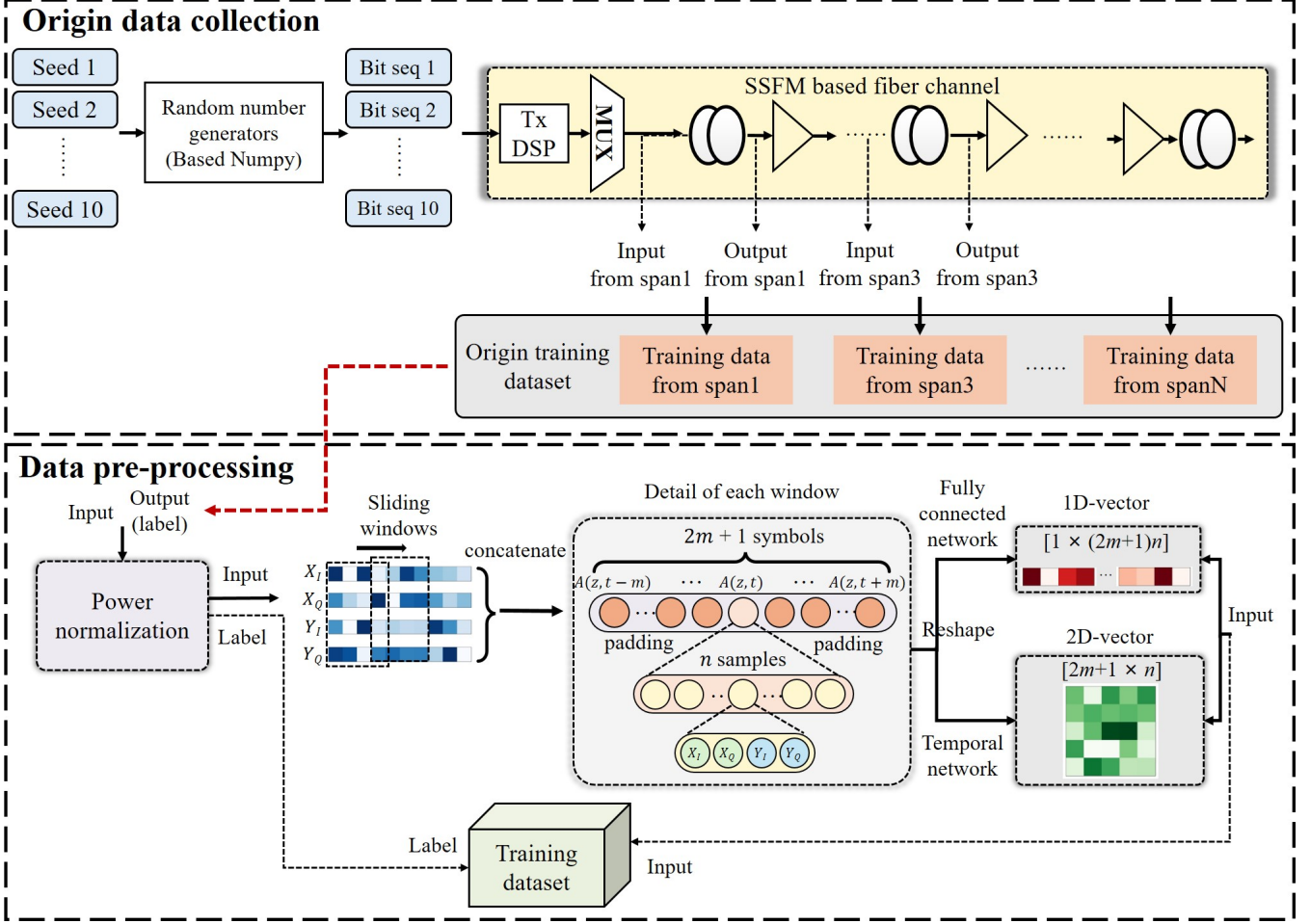


Fig. 2. The processing of dataset construction.

loss function to enhance model convergence by embedding physical constraints. The input of the trunk network includes distance and time coordinates, which can be differentiated automatically. Through a stacked-DeepONet architecture, it can be successfully applied to a fully-loaded C+L-band WDM system. The main advantage of neural operators is their superior generalization ability. The goal of neural operators is to approximate the mapping between function spaces, and once this mapping is learned, the parameterized operator can consistently locate the correct solution in the objective function space, regardless of changes in initial conditions. This generalization ability has proven effective for varying launch power in optical fiber channel modeling. Overall, neural networks with efficient structural designs, and neural operators with stronger generalization, have demonstrated distinct advantages in optical fiber channel modeling. Further research is needed to explore how to integrate the strengths of both approaches to enhance applications in this field.

B. Dataset construction

Before training the DL models, we need to construct the dataset, which includes two stages: original data collection and data pre-processing, as shown in Fig. 2. The original data is collected from SSFM-based simulation systems. To

mitigate overfitting and reduce pattern prediction by neural networks [74], [75], multiple random seeds are employed to generate diverse bit sequences through a NumPy-based random number generator. In this study, ten distinct random seeds are employed to generate the training dataset, and one different random seed is used to generate the testing dataset. Each generated bit sequence is mapped to the DP-16QAM constellation, producing sequences of 7680 symbols per polarization, which are then transmitted through an SSFM-based optical fiber channel. The data collection methods differ between overall and distributed schemes. In the overall scheme, a single DL model is employed to model the long-haul optical fiber channel, collecting waveform data only at transmission distances of 0 km and D km (the final transmission distance). On the contrary, the distributed scheme uses multiple cascaded DL models to model each fiber span individually. Thus, input and output data from various fiber spans are collected. In this study, the waveform data is collected from fiber spans [1, 3, 5, 7, 9] to enrich the training dataset, incorporating a variety of span input and output features, which enhances the model's performance for long-haul transmission [42]. ASE noise, caused by the EDFA, is introduced into the output signal after each fiber span transmission, contributing a random property to the input-to-output mapping. Only generative models,

such as CGAN, can handle random characteristics. Other neural networks, such as FCNN or BiLSTM, are typically capable only of fitting deterministic mappings and struggle with random features. To address this issue, we collect the output waveform before the EDFA introduces random noise, ensuring that the input-output mapping in the dataset contains only deterministic features.

After collecting original waveform data, data preprocessing is necessary to accelerate model convergence and adapt to different input format requirements across various DL models. For all DL models, the preprocessing step includes power normalization, sliding windows, and reshaping. Additionally, linear feature decoupling is necessary for the FDD scheme. The output signals are passed through simple linear compensation to eliminate CD, which can be described by the following equation:

$$A(z - L, \omega) = A(z, \omega) \exp\left(-i\frac{\beta_2}{2}\omega^2\right)(-L) \quad (5)$$

After linear compensation, the output signals contain only nonlinear characteristics. Then, power normalization is applied to facilitate model convergence by adjusting the input and output signals according to the following equation [25]:

$$\tilde{x} = x \cdot \sqrt{\frac{1}{\sum_{i=1}^{N_{ch}} P_i}}, \quad (6)$$

where N_{ch} represents the total number of the WDM channels, and P_i is the power of the i -th channel. Given that the dataset comprises complex signals with dual polarization (X and Y) and DL models are better at dealing with real number than complex ones. The complex signals are decomposed into two real-valued components: in-phase (I) and quadrature (Q) signals. At each time step, the real-valued signals of the two polarizations—denoted as X_I , X_Q , Y_I and Y_Q —are concatenated into a one-dimensional vector. To preserve accuracy, it is essential to account for inter-symbol interference (ISI) induced by CD when constructing the input data. The number of symbol affected by ISI is determined using the equation:

$$N_{ISI} = \frac{\Delta T}{\Delta t} = \frac{L\beta_2\Delta w}{1/S} = L\beta_2\Delta wS, \quad (7)$$

where N_{ISI} represents the number of symbols affected by ISI, ΔT is the temporal width affected by ISI, Δt is the time duration of one symbol, L is the transmission distance, $\Delta\omega$ is the spectrum width, and the S is the symbol rate. To account for ISI, adjacent symbols are included in the input data using a sliding window. The window length is adjusted based on the ISI strength, which varies with the symbol rate, spectrum width, and transmission distance. The input window consists of symbols at different times, represented as $[A(z, t - m), \dots, A(z, t), \dots, A(z, t + m)]$, where $A(z, t)$ is a one-dimensional vector aligned at distance z and time t , with dimension d . Here, m is the number of adjacent symbols, typically set as $(N_{ISI} - 1)/2$, ensuring accurate representation of CD effects. The FDD scheme employs a linear decoupling method, enabling the DL model to focus exclusively on fitting nonlinear characteristics. Inter-symbol correlations in residual nonlinearities are shorter than that caused by CD, due to

continuous signal power attenuation during fiber propagation. The nonlinear inter-symbol correlations can be approximated using the effective nonlinear length, expressed as:

$$L_{\text{eff}} = \frac{1}{\alpha}, \quad (8)$$

$$N_{NL} = L_{\text{eff}}\beta_2\Delta wS, \quad (9)$$

where L_{eff} presents the effective nonlinear length, and N_{NL} denotes the number of symbols affected by nonlinear inter-symbols correlations. Each symbol within input window comprises N sample points, with each sample point containing the four-dimensional signals X_I , X_Q , Y_I , Y_Q . Thus, the total dimension d of $A(z, t)$ is calculated as:

$$d = 4N_{SPS} = 4 * 4 * N_{ch} \quad (10)$$

where N_{SPS} is the samples per symbol (SPS) of SSFM, which is 4 times the channel number. Following the sliding window processing, the input window is reshaped to meet the specific input requirements of various DL models, including fully connected networks and temporal networks. For fully connected networks, such as GAN, FNO, and the branch net of DeepONet, the input is reshaped as a one-dimensional vector containing symbols from $2m + 1$ distinct time steps, represented as $[b, (2m + 1) * d]$, where b is the batch size. For temporal networks, such as BiLSTM and multi-head attention mechanism, the input is structured as a two-dimensional vector, expressed as $[b, 2m + 1, d]$, where the second dimension corresponds to different time steps, and the third dimension represents the dimension of each symbol. Additionally, the distance z and time t are considered as the inputs to the trunk net of DeepONet [43].

C. Training processing

After dataset construction, the next step is to train the DL models. The entire dataset is divided into training, validation, and test sets in a ratio of 8:2:1. The optimal model parameters are selected based on the test set results to avoid overfitting. The commonly used loss functions are the SL1 loss and MSE loss, defined as

$$Loss_{MSE} = \frac{\sum_{i=1}^{N_{\text{data}}} (\hat{y}_i - y_i)^2}{N_{\text{data}}}, \quad (11)$$

$$Loss_{SL1} = \frac{1}{N_{\text{data}}} \sum_{i=1}^{N_{\text{data}}} \begin{cases} 0.5(\hat{y}_i - y_i)^2 & \text{if } |\hat{y}_i - y_i| < 1 \\ |\hat{y}_i - y_i| - 0.5 & \text{otherwise} \end{cases}, \quad (12)$$

where N_{data} is the number of the data size, y and \hat{y} denote the outputs from SSFM and DL schemes, respectively. In this study, we choose SL1 as the loss function. The number of epochs is set at 1000. The Adam optimizer [76] is used with an initial learning rate (LR) of 5E-4, and the LR is adjusted using a cosine annealing schedule [77] for each epoch to improve training performance.

IV. THE ACCURACY EVALUATION METHOD FOR DL-BASED SCHEMES

We have introduced the classification and the training process of DL schemes. After training, it is important to evaluate the accuracy of DL models. This section reviews existing accuracy evaluation metrics, including NMSE, which reflects waveform errors, and constellations, GSNR, and Q-factor, which reflect transmission performance errors. Further, we find and analyze their potential limitations, including the difficulty in defining an acceptable NMSE threshold and the inconsistency between NMSE and Q-factor errors. To overcome the above shortcomings, we propose a DSP-assisted accuracy evaluation method to overcome these shortcomings in existing metrics, offering a fair and comprehensive benchmark for assessing accuracy and establishing a robust foundation for subsequent comparisons between various DL models in wideband systems.

A. The metrics for accuracy evaluation

Accuracy evaluation metrics for DL-based optical fiber channel modeling typically involve waveform errors and transmission performance errors. For waveform modeling schemes, waveform errors offer an intuitive means of accuracy comparison. These errors can be analyzed by examining deviations in waveform profiles and are quantitatively measured using the NMSE, defined as:

$$NMSE = \frac{\sum_{i=1}^{N_{\text{data}}} |\hat{y}_i - y_i|^2}{\sum_{i=1}^{N_{\text{data}}} |y_i|^2}, \quad (13)$$

When ASE noise from the EDFA is incorporated, the same random noise is applied to both SSFM and DL schemes during NMSE calculations to maintain consistency and avoid significant discrepancies in the NMSE values. Previous studies have established that an NMSE threshold below 0.02 indicates sufficiently accurate DL models [32].

In addition to waveform errors, transmission performance errors are crucial metrics in communication systems, used to assess whether DL schemes can serve as alternatives to SSFM and be applied in DSP algorithm design and system parameter optimization. To evaluate transmission performance, DSP algorithms are essential for compensating optical fiber channel impairments. Constellations are commonly used to analyze transmission performance, offering a visual representation of noise distribution by showing the deviation between the received constellation points and the transmitted constellation points. Quantitatively, the GSNR is calculated to evaluate the noise level of received signals. GSNR is defined as:

$$GSNR = 10 \log_{10} \left(\frac{P_s}{\mathbb{E}|rx - tx|^2} \right) = 10 \log_{10} \left(\frac{P_s}{P_{\text{ASE}} + P_{\text{NL}}} \right), \quad (14)$$

where rx and tx are the received and transmitted samples, respectively, P_s is the signal power, P_{ASE} is the ASE noise from the EDFA, and P_{NL} denotes the nonlinear noise introduced by optical fibers. Subsequently, demodulation is performed to calculate the bit error rate (BER) and Q-factor, defined as:

$$BER = \frac{N_{\text{error}}}{N_{\text{bits}}} \quad (15)$$

$$Q = 20 \log_{10} \left(\sqrt{2} \operatorname{erfc}^{-1}(2BER) \right), \quad (16)$$

where N_{error} is the number of erroneous bits, N_{bits} is the total number of bits, and $\operatorname{erfc}(x)$ is complementary error function. The Q-factor is derived as a logarithmic transformation of the BER, implying that identical Q-factor errors correspond to different BER errors under varying noise conditions. The accumulation of nonlinear and random noise varies across different transmission distances or WDM configurations. To ensure fair comparisons across different WDM configurations, extra noise are introduced at the receiver to keep BER and Q-factor values consistent across different configurations. This noise, applied to the received signals for both SSFM and DL schemes, is generated using the same random seed. In this study, the BER is maintained at 4E-2 for calculating the Q-factor, which is the 25% soft-decision forward-error-correction (SD-FEC) BER threshold [78].

B. The potential limitations of accuracy metrics

The metrics discussed in the previous subsection are widely employed to evaluate the accuracy of DL-based optical fiber channel waveform modeling, offering valuable insights into the performance differences between DL methods and SSFM. However, the interrelationships between these metrics have not been thoroughly examined. We find that Waveform errors do not directly correlate with transmission performance metrics, and, as a result, the NMSE threshold of 0.02 may not be universally adequate, especially in highly nonlinear systems. Additionally, the consistency between waveform errors and transmission performance errors may become problematic, particularly after long-haul transmission. In the following, we investigate these potential limitations and present illustrative examples to clarify these relationships.

1) **The acceptable NMSE threshold:** An NMSE threshold of 0.02 has been established as an acceptable benchmark for DL schemes in previous studies [32] and is widely adopted in subsequent research [33], [41]. To evaluate the suitability of this threshold under strong nonlinear conditions, we use FDD-BiLSTM as an example and test its performance in an 11-channel configuration with a transmission rate of 140 GBaud and a launch power of 8 dBm—approximately 2.5 dB higher than the optimal launch power and situated in the high nonlinear regime. First, waveform errors are assessed by examining the time-domain waveforms and NMSE values between FDD-BiLSTM and SSFM. Fig. 2(a) shows the time-domain waveforms and their NMSE at both 80 km and 400 km transmission, with NMSE values of 1.97E-3 and 1.94E-2, respectively—both of which fall below the accepted threshold of 0.02. Next, transmission performance is assessed for both FDD and SSFM to explore the relationship between the acceptable NMSE threshold and transmission performance errors. Fig. 2(b) displays the constellations of FDD and SSFM after linear DSP at 80 km and 400 km. The constellations of FDD exhibit less noise accumulation than SSFM, particularly due to nonlinear phase rotation associated with signal power. These results highlight that even when waveform distortions remain within the acceptable NMSE threshold, discrepancies in noise distribution can be significant. The primary reason

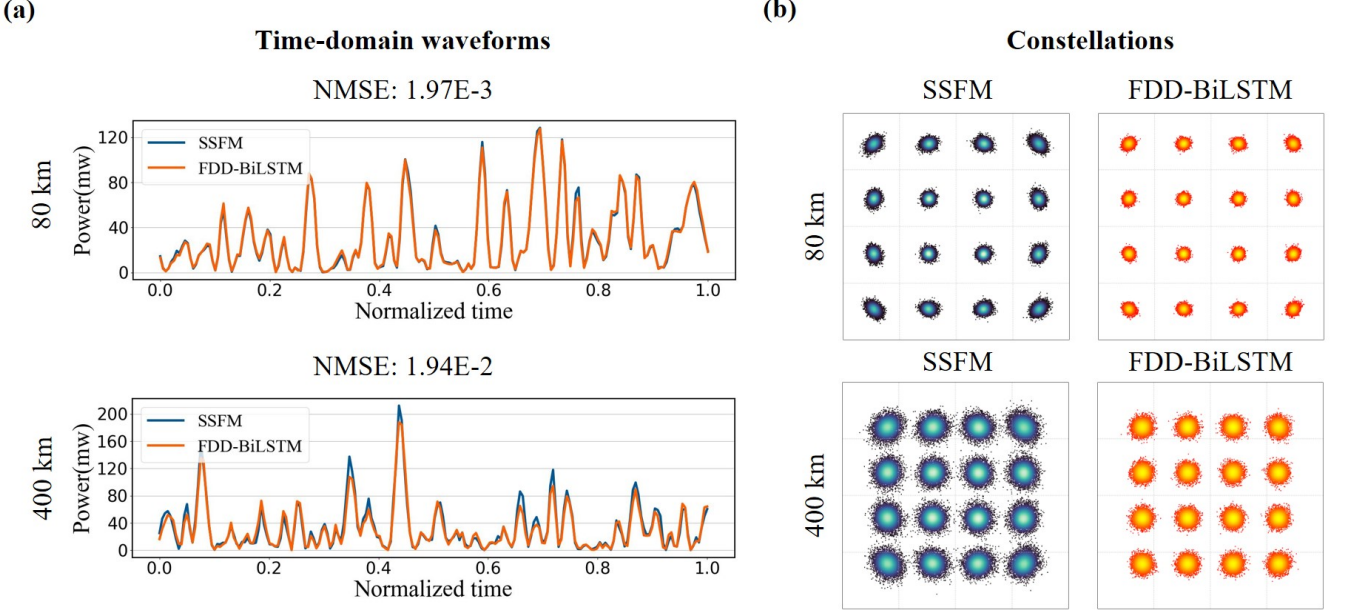


Fig. 3. Comparison of FDD-BiLSTM and SSFM at 80 km and 400 km. (a) Time-domain waveforms and NMSE values. (b) Constellations after linear DSP.

for this disparity lies in the fact that nonlinearity acts as a perturbation term [79], which minimally affects waveform distortions but significantly influences noise accumulation and transmission performance. Accurate modeling of both random and nonlinear noise is essential to reflect the actual behavior of the fiber channel and support applications such as nonlinear compensation algorithm design.

These findings indicate that the NMSE threshold of 0.02 is insufficient in certain scenarios with strong nonlinearities, and defining a universal NMSE threshold across varying scenarios remains challenging due to varying noise accumulation. Although establishing a universal NMSE threshold is difficult, NMSE continues to serve as a valuable relative metric for evaluating the accuracy of waveform-level modeling. Further accuracy evaluation should also incorporate transmission performance error to ensure that the model's accuracy meets the specific requirements of applications, such as using DL models for fast DSP algorithm optimization or link performance prediction.

2) *The inconsistency between waveform errors and transmission performance errors for distributed schemes:* Establishing a universal NMSE threshold is challenging, and further accuracy evaluation needs to incorporate transmission performance errors. However, transmission performance — as reflected by the Q-factor or GSNR—is a statistical metric influenced by various types of impairments in the received signals after long-haul transmission. These impairments include real, inherent linear and nonlinear effects captured by DL models, as well as artificial impairments introduced by model inaccuracies, such as iterative errors in distributed schemes. The impact of these impairments on transmission performance varies: some errors may improve performance, while others degrade it, and different types of errors dominate at different transmission distances. This results in fluctua-

tions in transmission performance and inconsistencies between waveform errors and transmission performance, complicating the evaluation process.

To investigate the influence of various types of impairments on the transmission performance of DL models and the inconsistency between transmission performance and waveform errors, we conduct a test using FDD-BiLSTM in a 3-channel WDM system with a transmission rate of 50 Gbaud and a launch power of 4 dBm—approximately 2.5 dB higher than the optimal launch power. To adjust the accuracy of FDD-BiLSTM, we vary the number of layers in BiLSTM, which is used for nonlinear effects modeling. The number of layers was set to 1 and 3. Increasing the number of layers enhances the model's nonlinear fitting capacity, leading to higher model accuracy. Both models are trained on the same dataset with identical hyperparameters. First, waveform errors are evaluated using NMSE. Fig. 4(a) shows the NMSE curves over a 1200 km transmission range for both the 1-layer and 3-layer BiLSTM models. The 3-layer BiLSTM achieves consistently lower NMSE values than the 1-layer BiLSTM across a 1200 km transmission distance, demonstrating its superior waveform modeling capacity due to its deeper network and enhanced ability to capture nonlinearities. Next, transmission performance errors are assessed using the Q-factor after linear DSP. The Q-factor error is calculated as the difference between the Q-factor of the SSFM and that of the DL models, expressed as:

$$Q_{\text{error}} = Q_{\text{SSFM}} - Q_{\text{DL}}, \quad (17)$$

Fig. 4(b) shows that Q-factor errors for the 1-layer BiLSTM remain below 0.1 dB over the 1200 km transmission range, whereas Q-factor errors for the 3-layer BiLSTM increase with distance, peaking at 0.33 dB. These results indicate that the 1-layer BiLSTM more closely matches the transmission performance of SSFM, despite its inferior waveform modeling

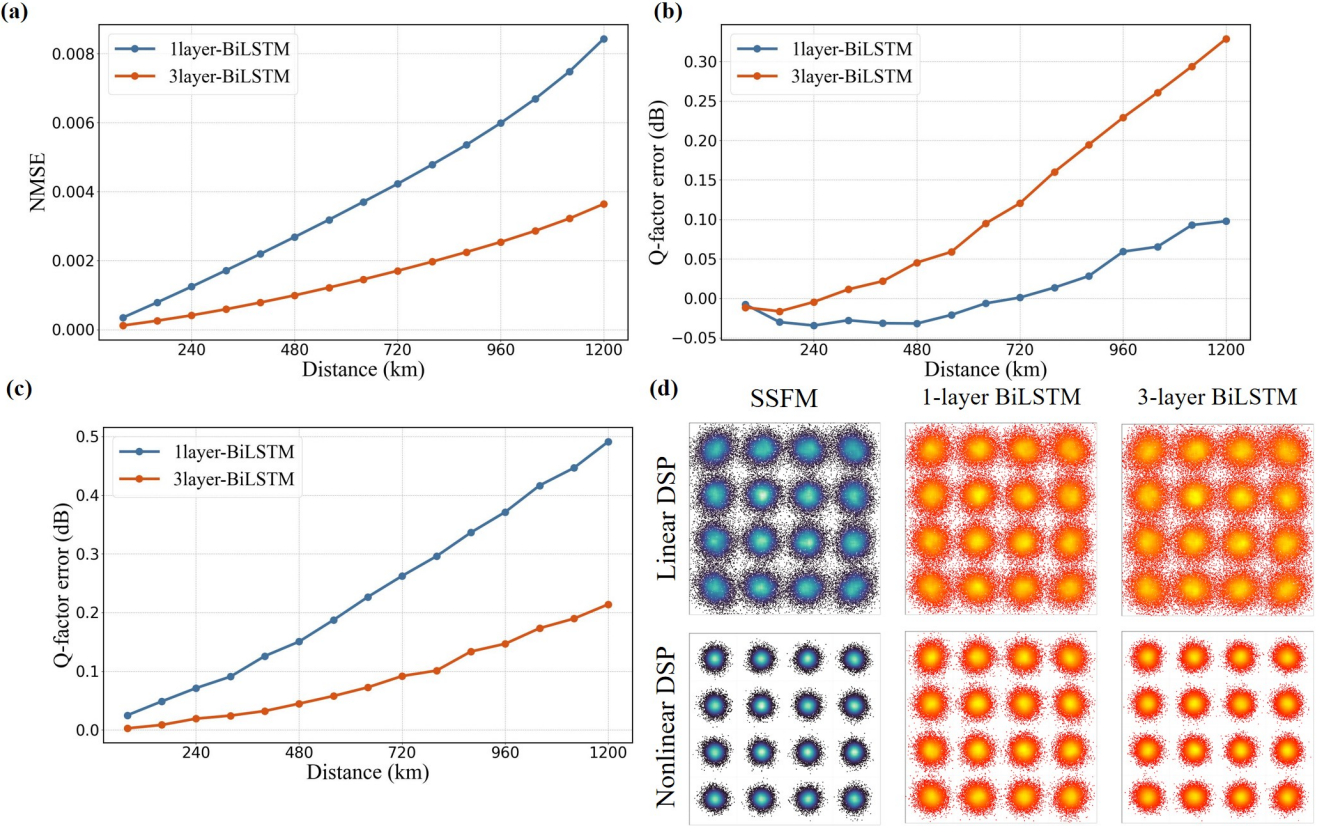


Fig. 4. Comparison of 1-layer and 3-layer BiLSTM between SSFM. (a) NMSE curve covering 1200 km. (b) Q-factor error after linear DSP processing covering 1200 km. (c) SNR error after nonlinear DSP processing covering 1200 km. (d) Constellations after linear and nonlinear DSP processing at 1200 km.

capacity. This inconsistency between waveform errors and transmission performance complicates determining which DL model is truly more accurate.

The inconsistency between waveform and transmission performance errors arises from the fact that the transmission performance of received signals modeled by DL schemes is affected by two types of impairments: the linear and nonlinear channel effects modeled by DL models, and iterative errors due to the cascading of multiple DL models. The channel effects modeled by DL models differ from those of the SSFM, making the nonlinear noise present in signals modeled by DL models lower than that of the SSFM. This lower nonlinear noise results in better transmission performance and higher Q-factor values, causing negative Q-factor errors. These Q-factor errors, caused by differences in channel effect modeling between DL models and the SSFM, are termed channel effect modeling errors. Additionally, iterative errors arise from cascading multiple DL models to achieve long-haul transmission in distributed schemes. Errors from earlier models propagate to subsequent ones, leading to error accumulation over the transmission distance. These iterative errors degrade the transmission performance of DL-modeled signals compared to SSFM results, resulting in positive Q-factor errors. Over long-haul transmission, both types of errors occur simultaneously: channel effect modeling errors drive negative Q-factor errors, while iterative errors lead to positive Q-factor errors, causing fluctuations in transmission performance and inconsistencies

between waveform and transmission performance errors.

Next, we further examine the fluctuations in transmission performance by analyzing the change in Q-factor errors over long-haul transmission. We compare the results for the 1-layer and 3-layer BiLSTM models. Fig. 4(b) shows that, at short transmission distances, the Q-factor errors for the 1-layer BiLSTM are negative, indicating the dominance of channel effect modeling errors, as iterative errors have not yet accumulated significantly. As the transmission distance increases, iterative errors accumulate and begin to dominate, degrading the Q-factor of the 1-layer BiLSTM and shifting its Q-factor errors into the positive region. At 1200 km, the combined effects of channel effect modeling errors and iterative errors result in a Q-factor error of only 0.1 dB for the 1-layer BiLSTM, but this does not indicate higher accuracy. In contrast, the Q-factor errors for the 3-layer BiLSTM remain positive throughout most of the transmission range, except for the initial spans. This occurs because the higher modeling capacity of the 3-layer BiLSTM reduces channel effect modeling errors, allowing iterative errors to dominate across the entire transmission distance. The dominance of iterative errors causes the Q-factor errors for the 3-layer BiLSTM to continually increase with transmission distance. These results reveal that lower Q-factor errors do not necessarily indicate superior accuracy, as they may result from the coincidental cancellation of channel effect modeling errors and iterative errors over long-haul transmission. Although these findings

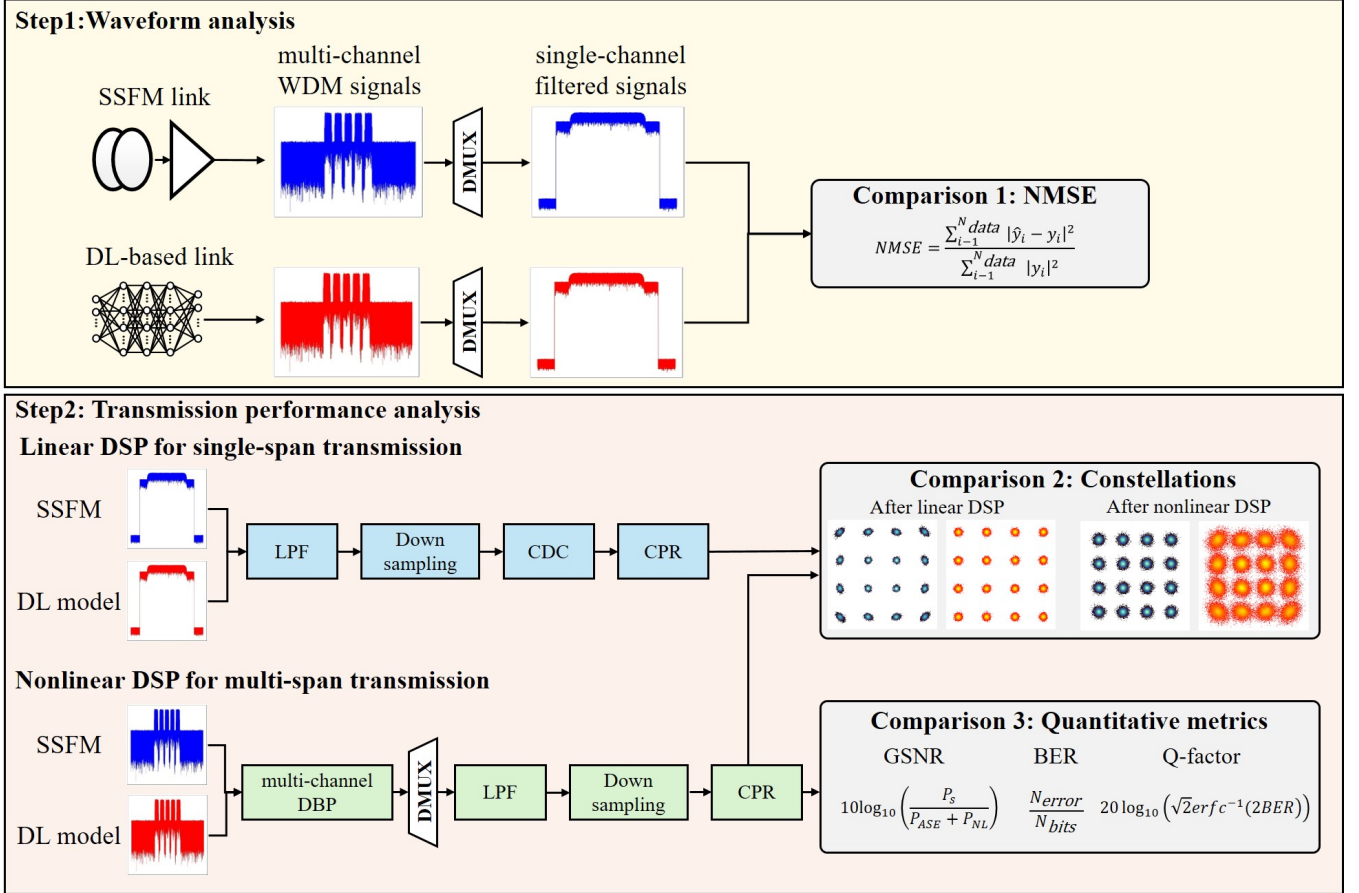


Fig. 5. The specific flow of DSP-assisted accuracy evaluation method.

are demonstrated using the FDD-BiLSTM scheme, we believe that this inconsistency phenomenon will also arise in other distributed DL schemes. Regardless of the specific distributed DL model, both channel effect modeling errors and iterative errors will occur after long-haul transmission, leading to fluctuations in Q-factor results. Therefore, an additional accuracy metric is necessary to effectively reflect transmission performance and ensure consistency with waveform errors during long-haul transmission.

3) **DSP-assisted accuracy evaluation method:** We have discussed the limitations of existing accuracy metrics, including the difficulty in defining a universally accepted NMSE threshold and the inconsistencies between waveform errors and transmission performance errors after linear DSP. To address these limitations and establish a reliable accuracy evaluation method for comprehensively comparing DL models, we propose a DSP-assisted accuracy evaluation method. This approach incorporates both waveform errors and transmission performance errors, utilizing nonlinear DSP algorithms to eliminate Q-factor fluctuations observed after linear DSP and to achieve consistency between waveform errors and transmission performance errors. The DSP-assisted evaluation method consists of two stages: waveform analysis and transmission performance analysis, as illustrated in Fig. 5.

In the first stage, waveform analysis, full-field multi-channel WDM signals from both SSFM-based and DL-based optical

fiber links are obtained and demultiplexed to extract filtered single-channel signals. The contour shapes of the waveforms in both the time and frequency domains provide an intuitive means for waveform analysis. Additionally, the NMSE of the filtered single-channel signals is calculated quantitatively to exclude the influence of out-of-band noise on accuracy. NMSE values obtained during testing directly correspond to the loss function used during the training process, making NMSE an effective and relative metric for assessing accuracy. Lower NMSE values indicate greater accuracy in waveform modeling capacity.

The second stage, transmission performance analysis, focuses on comparing transmission performance according to constellations and Q-factor errors. Linear effects of the fiber channel are relatively easy to represent by a physical model and can be effectively compensated by advanced linear DSP, while the representation of nonlinear effects is more complex, making it the primary focus of DL modeling. Therefore, validating the modeling capacity for nonlinear effects is a critical part of the accuracy evaluation process. The modeling accuracy of nonlinear effects can be assessed by analyzing nonlinear phase rotations in the constellations after linear DSP and the nonlinear noise accumulation reflected by Q-factor degradation. Since transmission performance after linear DSP is influenced by the interaction between channel effect modeling errors and iterative errors, results from linear DSP are valid

primarily for short-distance transmissions, where the influence of iterative errors is minimal. Therefore, constellations after linear DSP following one-span fiber transmission serve as a metric for analyzing nonlinear phase rotations. For long-haul transmission performance analysis, the fluctuations in Q-factor need to be addressed. We propose incorporating a nonlinear compensation algorithm—multi-channel DBP—to resolve this limitation. This algorithm compensates for both linear and nonlinear impairments by inversely solving the NLSE. Unlike traditional single-channel DBP, multi-channel DBP operates on full-field multi-channel WDM signals, enabling joint compensation of intra-channel and inter-channel nonlinearities. The parameters of multi-channel DBP are set to match those of SSFM exactly: gamma is set to $1.3/(W \cdot km)$, and the step size configuration uses the maximum phase rotation method with the maximum phase rotation of 0.005. This configuration ensures that the multi-channel DBP algorithm mirrors the inverse process of SSFM and fully compensates the nonlinear impairments. There are two advantages to incorporating multi-channel DBP. On one hand, the inverse compensation process allows us to evaluate whether the forward nonlinear modeling of DL models is consistent with SSFM. On the other hand, it addresses the fluctuations of Q-factor after linear DSP, which arise from the fact that nonlinear modeling errors and iterative errors impact the Q-factor in opposite directions—improving it and degrading it respectively. DL models often exhibit underfitting of nonlinear effects compared to SSFM, leading to “compensation overflow” during full inverse compensation. This happens because DBP works by calculating the NLSE inversely, which can introduce additional nonlinear impairments. These additional impairments resemble the effects of insufficient forward modeling, except that the nonlinear phase rotates in the opposite direction. After applying multi-channel DBP, the forward nonlinear modeling errors are transferred to additional impairments, which degrade the Q-factor similarly to iterative errors. This eliminates the fluctuation of the Q-factor and ensures more stable and accurate performance evaluation.

To validate the effectiveness of applying the multi-channel DBP algorithm, we compare the results of SSFM, 1-layer BiLSTM, and 3-layer BiLSTM models. Fig. 4(d) shows constellations after both linear and nonlinear DSP at an 800 km transmission distance. After linear DSP, constellations for both BiLSTM models closely resemble those of SSFM, making their performance difficult to distinguish. However, after nonlinear DSP, the 3-layer BiLSTM constellations align more closely with SSFM, while the 1-layer BiLSTM exhibits significant deviations and pronounced nonlinear impairments. These observations validate that the multi-channel DBP algorithm effectively transforms insufficient forward nonlinear modeling into additional nonlinear impairments. Further validation is provided by analyzing Q-factor errors. Fig. 4(c) illustrates Q-factor errors after nonlinear DSP over a 1200 km transmission range. The 1-layer BiLSTM exhibits higher Q-factor errors, peaking at 0.5 dB, compared to the 3-layer BiLSTM, which has a maximum error of 0.21 dB. These results indicate that the 3-layer BiLSTM more accurately mirrors the nonlinearity of SSFM. As shown in Fig. 4(a) and (c), the results of

NMSE and Q-factor errors after nonlinear DSP show the same trend, demonstrating that the multi-channel DBP algorithm effectively resolves the fluctuations of Q-factor after linear DSP and achieves consistency between waveform errors and transmission performance errors over long-haul transmission.

The DSP-assisted accuracy evaluation method, which integrates waveform errors and transmission performance errors, provides a comprehensive performance analysis of DL models. It incorporates multi-channel DBP to resolve the issue of fluctuations of Q-factor after linear DSP and achieves consistency between waveform errors and transmission performance errors, thus providing a fair and comprehensive benchmark for comparing various DL models in the next section.

V. COMPARISON OF DL-BASED SCHEMES

DL-based optical fiber channel waveform modeling schemes have demonstrated comparable accuracy with significantly reduced complexity compared to traditional SSFM. In Section III, we have introduced different types of DL schemes and their training methodologies. Currently, DL models are primarily applied to single-channel and few-channel WDM systems, or simplified wideband WDM configurations, with their performance in wideband scenarios remaining inadequately explored. Additionally, there is a lack of fair and comprehensive comparison of DL models under unified conditions and standards. In this section, we present a comprehensive comparison of different types of DL schemes based on the DSP-assisted accuracy evaluation methods proposed in Section IV. To provide a more thorough analysis of their performance, the comparisons begin with simpler scenarios, progressing from few-channel and low-rate to multi-channel and high-rate wideband configurations. By selecting progressively more challenging scenarios, we aim to identify the best-performing schemes and reveal their application potential in wideband environments. Furthermore, based on results exhibited in wideband scenarios, we analyze the challenges faced by DL schemes, considering both more intricate linear and nonlinear effects, as well as higher sampling rates. This analysis provides valuable insights that will inform the future optimization of DL models for improved performance in wideband channel waveform modeling.

A. Comparisons in few-channel and low-rate WDM systems

DL schemes have demonstrated outstanding performance in few-channel WDM systems. Therefore, the first scenario for comparison is set to a 5-channel WDM configuration. The transmission rate is set at 50 Gbaud, with a launch power of 4 dBm per channel, creating a highly nonlinear scenario that demands stronger nonlinear modeling capacity of DL models. To provide a thorough comparison of DL approaches, the comparison is divided into two parts based on the classification of schemes in Section III, including overall versus distributed methods and pure-data driven versus data-physics hybrid-driven methods.

1) **Overall schemes vs. distributed schemes:** We compare the performance of both overall and distributed schemes. Specifically, the models compared include overall-BiLSTM

TABLE III
THE PARAMETERS OF DL MODELS FOR COMPARISON BETWEEN OVERALL AND DISTRIBUTED SCHEMES.

	Overall-CGAN		Overall-BiLSTM	Distributed-BiLSTM
	Generator	Discriminator		
Input size	13200	2	Input size	80
Hidden layer	4	4	Layers	3
Hidden size	[52600,6575,3287,1643,80]	[52640,6580,3290,1645,1]	Hidden size	80
Output size	80	20	Time steps	657

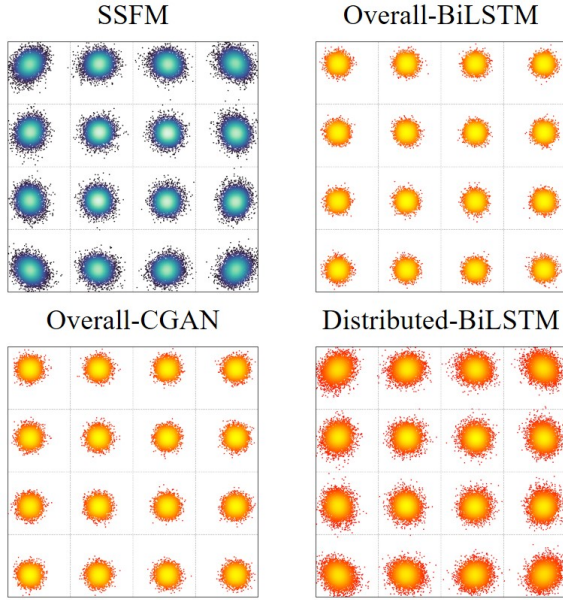


Fig. 6. Constellations of SSFM, overall-CGAN, overall-BiLSTM and distributed-BiLSTM at 320 km transmission.

TABLE IV
PERFORMANCE COMPARISON OF OVERALL AND DISTRIBUTED SCHEMES AT 800 KM TRANSMISSION.

Scheme	NMSE	Q-factor error(dB)
Overall-BiLSTM	0.0133	0.53
Overall-CGAN	0.0151	0.67
Distributed-BiLSTM	0.0011	0.16

[32], overall-CGAN [33], and distributed-BiLSTM. The parameters of these DL models are listed in Table III. The overall schemes utilize a single network to model the entire 320 km fiber link, while the distributed schemes employ four networks with identical parameters to cascade and achieve the same distance transmission. To address the ISI effects caused by CD accumulation over distances, the window length for distributed schemes is set at 211 symbols, while for overall schemes, it is 4 times that of the distributed schemes (844 symbols) due to longer CD accumulation.

To compare the performance between distributed schemes and overall schemes, we first examine their waveform modeling capabilities. The NMSE for each scheme at a transmission

distance of 320 km is presented in Table IV. Here, the NMSE is 0.0133 for overall-BiLSTM and 0.0151 for overall-CGAN, whereas the distributed-BiLSTM achieves a significantly lower NMSE of 0.0011. This indicates a more precise waveform modeling capability of the distributed schemes. Further analysis of transmission performance is conducted by examining the constellations after linear DSP, as shown in Fig. 6. The shapes of the constellations from overall schemes are dissimilar to that of SSFM, suggesting their inability to adequately represent both the random and nonlinear noise characteristics of the fiber link. Additionally, the Q-factor error after nonlinear DSP for overall-BiLSTM is 0.53 dB and 0.67 dB for overall-CGAN, whereas while that of the distributed-BiLSTM is only 0.16 dB, indicating a significant performance gap between overall schemes and SSFM.

The excellent results in waveform errors and transmission performance errors for distributed-BiLSTM highlight the better modeling capacity of distributed schemes. The BiLSTM is a deterministic model, which is inherently limited in handling random features. This limitation makes overall-BiLSTM particularly unsuitable for modeling long-haul fiber links with random noise between each fiber span. As a generative model, overall-GAN can learn random distributions but faces challenges in achieving convergence in multi-channel WDM systems due to the adversarial training process [69], [70]. In contrast, distributed schemes, which individually model the channel effects of each span, simplify the linear and nonlinear effects accumulated with the transmission distance, thus enhancing accuracy. Meanwhile, the random noise between each span can be directly modeled by a Gaussian distribution, eliminating the need for DL models to learn these random features. Therefore, distributed schemes are highly suitable for long-distance, multi-channel WDM systems and represent the main technical approach for future research.

2) **Pure data-driven schemes vs. data-physic hybrid-driven schemes:** Distributed schemes offer notable advantages in accuracy and flexibility in handling random noise, making them the preferred design in recent DL approaches. Therefore, the next comparison employs only distributed schemes. This section contrasts pure data-driven methods and data-physics hybrid-driven methods, involving both neural networks and neural operators. The pure data-driven schemes include BiLSTM, Multi-head Attention, FNO, and DeepONet, while the data-physics hybrid-driven scheme is represented by FDD-BiLSTM. These schemes have shown excellent results in few-channel WDM systems. Pure data-driven schemes model both

TABLE V
THE PARAMETERS OF DL MODELS FOR COMPARISON BETWEEN PURE DATA-DRIVEN AND DATA-PHYSIC HYBRID-DRIVEN SCHEMES.

DeepONet			FNO	
Branch Net		Trunk Net		
Input size	13200	2	Input size	13200×1
Hidden layer	4	4	Fourier layer	4
Hidden size	[6600,3300,1650,825,412]	[256,256,256,256,256]	Hidden dimension	16
Output size	80	20	Fourier mode	6600
BiLSTM		FDD-BiLSTM	Multi-head Attention	
Input size	80	80	Input size	80
Hidden size	80	80	Hidden size/FNN size	80/320
Layers	3	3	Layers	3
Time step	165	45	Time step	165

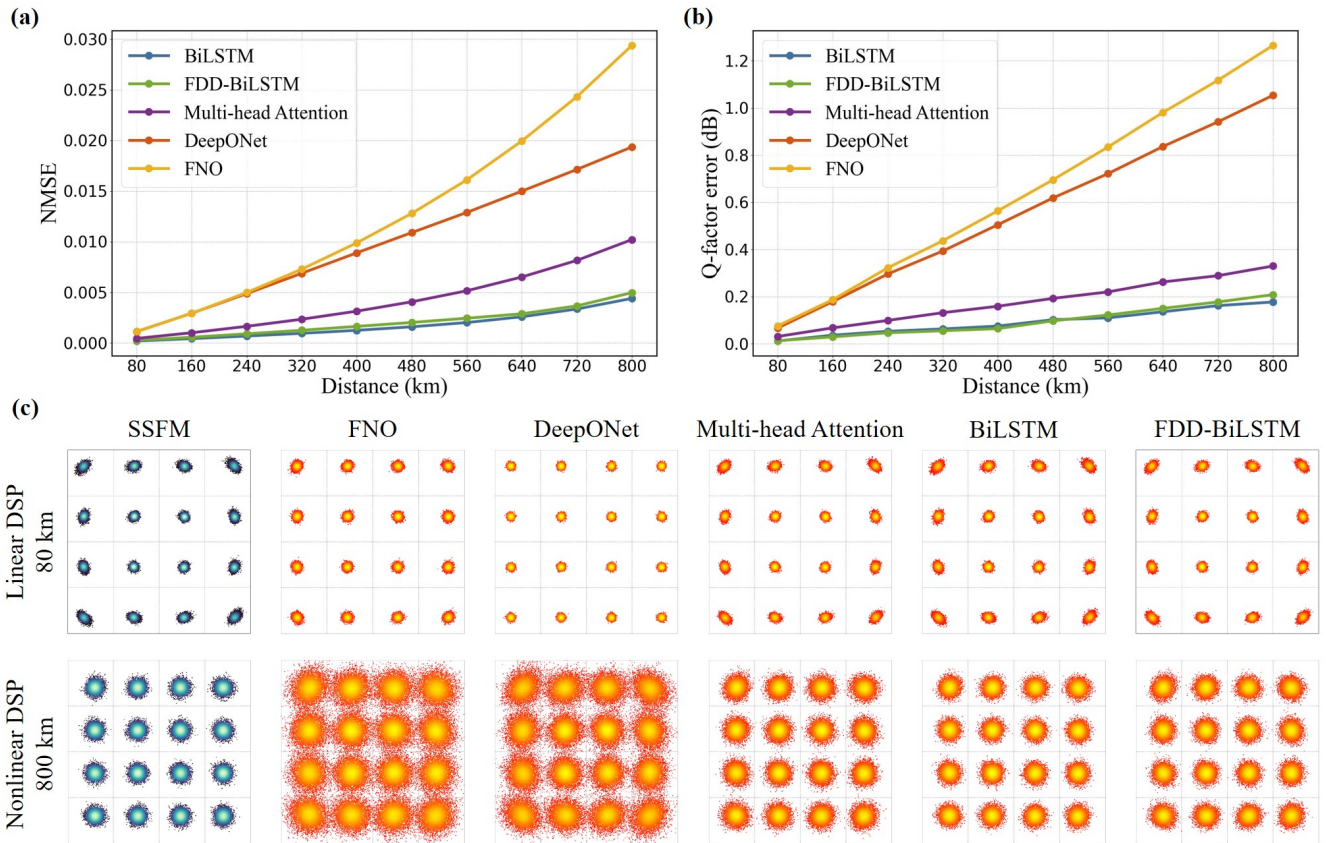


Fig. 7. Comparison of SSFM and DL-based schemes, including pure data-driven schemes and data-physic hybrid-driven schemes. (a) Time-domain waveform of SSFM and DL-based schemes at 800 km. (b) NMSE curve of DL-based schemes covering 800 km. (c) Q-factor error curve after nonlinear DPS processing between SSFM and DL-based schemes. (d) Constellations after linear DSP processing of SSFM and DL-based schemes at 80 km and 800km.

linear and nonlinear effects, while the FDD-BiLSTM focuses on nonlinear effects due to linear decoupling. For accurately modeling linear effects, the pure data-driven schemes require a longer input window to account for ISI, while the input window length of FDD-BiLSTM is reduced because the nonlinear inter-symbol correlations are shortened, as determined by equations (8) and (9). Therefore, pure data-driven schemes utilize an input window of 165 symbols (82+1+82), whereas

the data-physic hybrid-driven scheme requires only 45 symbols (22+1+22). Other model parameters are summarized in Table V.

To evaluate accuracy, each DL model is tested over 10 iterations for an 800 km transmission distance and compared to traditional SSFM. Waveform errors are assessed using NMSE. As shown in Fig. 7(a), both FDD-BiLSTM and BiLSTM exhibit excellent waveform modeling capabilities, with NMSE

values below 5E-3 over the entire 800 km transmission. Multi-head Attention performs slightly worse, with NMSE values just below 1E-2, indicating a slight accuracy drop compared to BiLSTM and FDD-BiLSTM. FNO and DeepONet exhibit larger discrepancies, with NMSE values of 2.94E-2 and 1.94E-2, respectively, at 800 km. Notably, the NMSE of FNO is six times higher than that of FDD-BiLSTM at 800 km transmission, indicating significant waveform distortion. The overall waveform modeling accuracy ranks as follows: FDD-BiLSTM \approx BiLSTM < Multi-head Attention < DeepONet < FNO.

The transmission performance is evaluated through constellations and Q-factor errors. To analyze the performance after single-span transmission, the first row of Fig. 7(c) presents the constellations of the DL models and SSFM at 80 km transmission after linear DSP. The constellation of SSFM shows clear nonlinear phase rotation due to high launch power (4.0 dBm). The constellations of BiLSTM, FDD-BiLSTM, and Multi-head Attention display similar nonlinear phase rotations, closely resembling SSFM. However, FNO and DeepONet exhibit Gaussian-like distributions, ignoring nonlinear phase rotation, indicating their worse nonlinear fitting capacity. To further evaluate transmission performance at long-haul transmission, the second row of Fig. 7(c) exhibits the constellations at 800 km transmission after nonlinear DSP. After multi-channel DBP processing, the SSFM constellation shows effective compensation results for linear and nonlinear impairments. The constellations of FDD-BiLSTM, BiLSTM, and Multi-head Attention exhibit similar compensation results. Multi-head Attention shows a little additional nonlinear noise due to its underfitting of nonlinearities. In contrast, constellations of FNO and DeepONet exhibit substantial additional noise induced by multi-channel DBP, indicating severe underfitting of nonlinearities. Subsequently, to quantitatively assess transmission performance, the Q-factor errors after nonlinear DSP between DL models and SSFM across 800 km transmission are presented in Fig. 7(b). Q-factor errors for all DL models increase with transmission distance, consistent with NMSE trends, due to error accumulation. BiLSTM and FDD-BiLSTM show nearly identical Q-factor errors, with a maximum error of around 0.2 dB after 800 km transmission, indicating excellent transmission performance compared to SSFM. Multi-head Attention performs slightly worse, with a maximum Q-factor error of 0.33 dB after 800 km transmission. FNO and DeepONet show rapid increases in Q-factor errors, reaching 1.27 dB and 1.05 dB, respectively, indicating substantial performance gap compared to SSFM.

Results from NMSE, constellations and Q-factor errors show good consistency, validating the effectiveness and fairness of the DSP-assisted accuracy evaluation method. The accuracy ranking of DL schemes, based on both NMSE and Q-factor, is as follows: FDD-BiLSTM \approx BiLSTM < Multi-head Attention < DeepONet < FNO. The superior performance of FDD-BiLSTM, BiLSTM, and Multi-head Attention can be attributed to their temporal design through recurrent structures and multi-head self-attention mechanisms, which efficiently capture nonlinear effects with temporal correlations. FNO and DeepONet, which mainly rely on fully

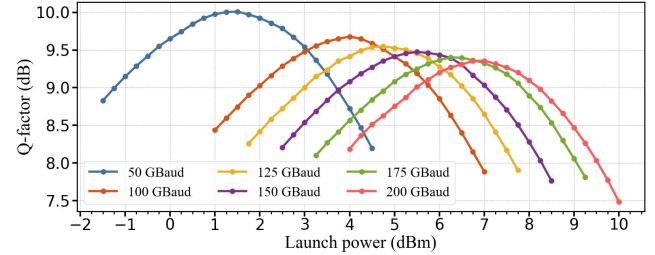


Fig. 8. Launch powers versus Q-factor at various symbol rates.

TABLE VI
LAUNCH POWERS AT VARIOUS SYMBOL RATES

Symbol rate (Gbaud)	Optimal launch power (dBm)	Testing launch power (dBm)
50	1.5	4.0
100	4.0	6.5
125	4.75	7.25
150	5.5	8.0
175	6.25	8.75
200	7.0	9.5

connected and convolutional structures to capture features, perform well in single-channel systems but struggle in 5-channel WDM systems. The increased ISI length and complex coupling of linear and nonlinear effects in 5-channel configurations degrade their accuracy. Additionally, fully connected structures face challenges in training and convergence due to the longer input vector (165 symbols concatenated into a one-dimensional input with a dimension of 13200). Temporal models like BiLSTM and Multi-head Attention process two-dimensional inputs, with rows representing symbols at different times and columns representing the sum of sampling points from four-dimension signals. These structures process the two-dimension input step-by-step through recurrent or self-attention units, avoiding the problem that fully connected networks face with excessively long one-dimensional inputs. Temporal network architectures are more suitable for addressing signals with longer inter-symbol correlations, thus outperforming FNO and DeepONet in multi-channel scenarios.

B. Comparisons in WDM systems with more-channel and higher-rate

In a 5-channel WDM configuration, BiLSTM and FDD-BiLSTM demonstrate comparable accuracy in waveform and transmission performance. To further differentiate their capabilities, we evaluate their performance in more complex WDM scenarios with more channels and higher rate. These test cases include: a 13-channel WDM system with a 50 Gbaud symbol rate and 4.0 dBm launch power, and a 5-channel WDM system with a 100 Gbaud symbol rate and 6.5 dBm launch power. The launch power for the 100 Gbaud case is increased to 6.5 dBm to match the higher optimal launch power due to the higher symbol rate. The trend of the optimal launch powers with symbol rates is shown in Fig. 8. The specific

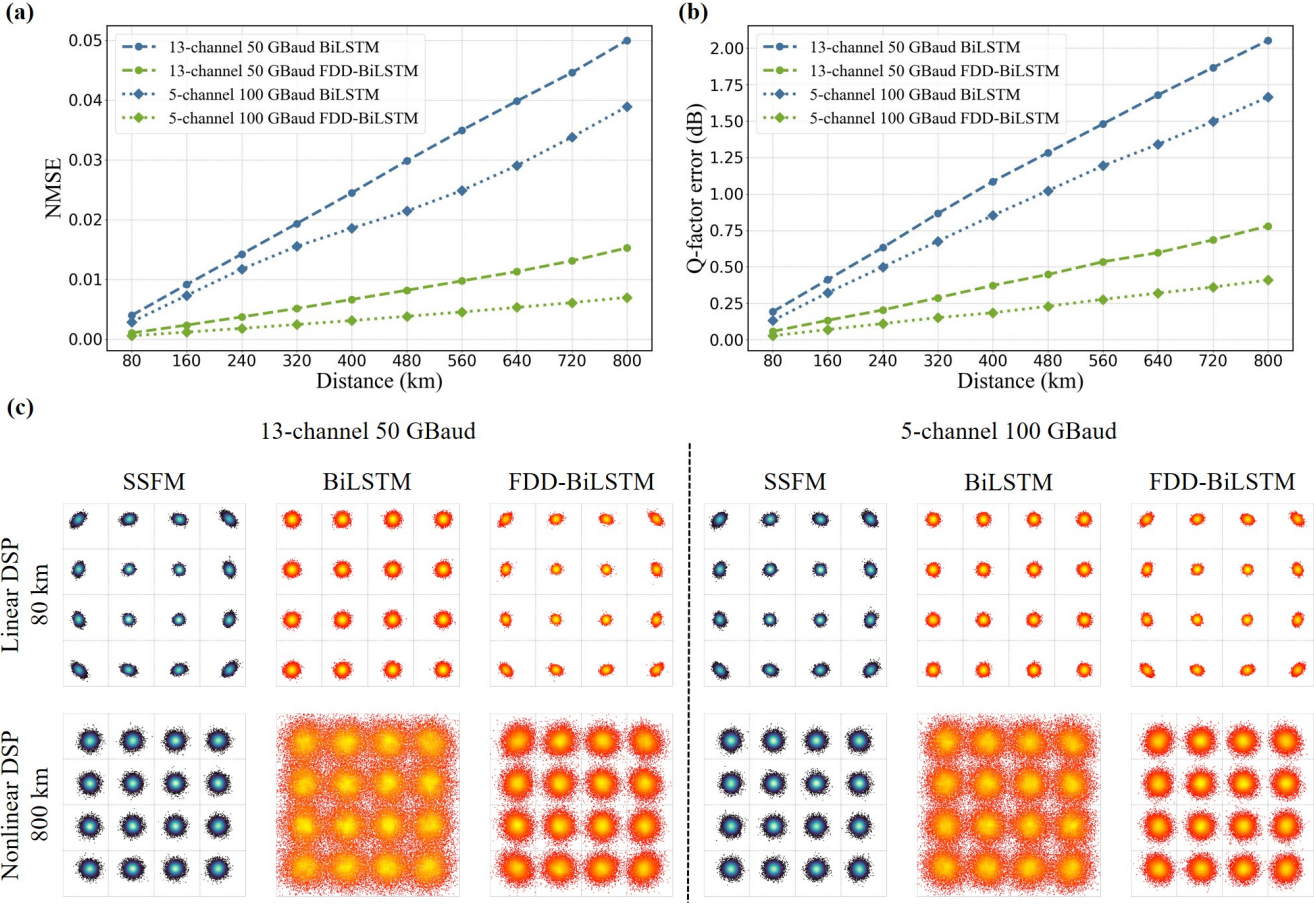


Fig. 9. Comparison of SSFM and FDD under 13-channel with 50 GBaud and 5-channel with 100 GBaud. (a) NMSE curve of FDD covering 800 km. (b) Q-factor errors curve after nonlinear DPS between SSFM and FDD. (c) Constellations after linear DSP at 80 km and after nonlinear DSP at 800 km of SSFM and FDD.

configurations of the optimal launch power and test launch power for different symbol rates are shown in Table VI. In these scenarios, the length of ISI and nonlinear inter-symbol correlations increases due to the wider spectrum and higher symbol rate, as determined by formulas (8) and (9). Therefore, the input window length is set to 427 and 117 symbols for BiLSTM and FDD-BiLSTM in the 13-channel 50 GBaud case, and 601 and 163 symbols in the 5-channel 100 GBaud case.

Both FDD-BiLSTM and BiLSTM are tested over 10 iterations for an 800 km transmission. NMSE curves over the 800 km transmission are shown in Fig. 9(a). In both WDM configurations, FDD-BiLSTM consistently outperforms BiLSTM, achieving lower NMSE values across the 800 km transmission. In the 13-channel 50 GBaud case with 800 km transmission, FDD-BiLSTM achieves a maximum NMSE of 1.53E-2, compared to BiLSTM's 5E-2, resulting in an NMSE difference of 3.47E-2. Similarly, in the 5-channel 100 GBaud case, FDD-BiLSTM achieves a maximum NMSE of 7E-3, significantly lower than BiLSTM's 3.89E-2. These results highlight superior waveform modeling accuracy of FDD-BiLSTM in WDM configurations with more channels and higher rates. The transmission performance is evaluated using constellations and Q-factor. The first row of Fig. 9(c) shows that the constellation of FDD-BiLSTM exhibits ob-

vious nonlinear phase rotation, similar to SSFM, indicating its effective nonlinear modeling capacity. Conversely, the constellation of BiLSTM displays Gaussian-like distributions, ignoring nonlinear phase rotation, exposing its limitations in nonlinear modeling. The second row of Fig. 9(c) shows constellations after 800 km transmission with nonlinear DSP. After multi-channel DBP, the constellations of SSFM show effective compensation for linear and nonlinear impairments. However, the constellations of FDD-BiLSTM and BiLSTM show additional nonlinear impairments, with the additional impairments of BiLSTM being particularly obvious, rendering BiLSTM ineffective for long-haul transmission. Furthermore, we quantitatively evaluate Q-factor errors. Fig. 8(b) illustrates the Q-factor errors after nonlinear DSP align with NMSE trends, as shown in Fig. 8(a). In the 13-channel, 50 GBaud case, FDD-BiLSTM achieves a Q-factor error of 0.78 dB after 800 km transmission, compared to 2.05 dB for BiLSTM. Similarly, in the 5-channel, 100 GBaud case, FDD-BiLSTM achieves a Q-factor error of 0.41 dB, while BiLSTM reaches 1.67 dB. The lower Q-factor errors of FDD-BiLSTM highlight its stronger modeling capacity compared to BiLSTM in WDM configurations with more-channel and higher-rate.

FDD-BiLSTM consistently outperforms BiLSTM, which is attributed to its data-physics hybrid-driven design. FDD-

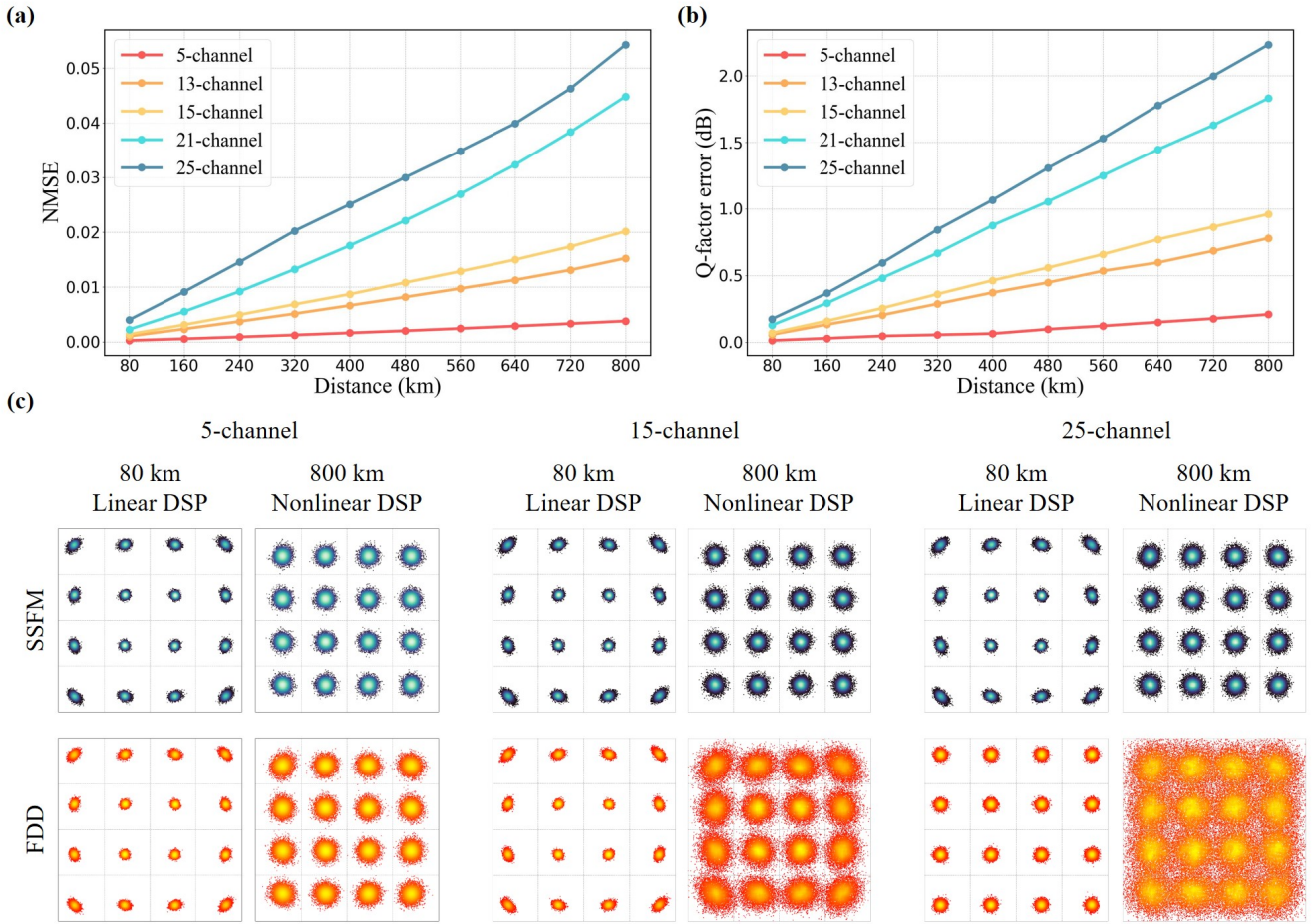


Fig. 10. The results of FDD-BiLSTM applied in more-channel WDM systems. (a) NMSE curve of different number of channels covering 800 km transmission. (b) Q-factor error curve after nonlinear DSP processing between FDD-BiLSTM and SSFM of different number of channels covering 800 km transmission. (c) Constellations after linear DSP processing of FDD-BiLSTM and SSFM of different number of channels at 80 km and 800 km transmission.

BiLSTM separates optical channel characteristics into linear and nonlinear components. Physical models are employed for modeling the linearity, ensuring high linear modeling accuracy across diverse WDM configurations. The DL model only focuses exclusively on modeling residual nonlinearities, simplifying the fitting process, particularly in more complex scenarios with stronger nonlinear effects. Additionally, FDD-BiLSTM requires a shorter input window than BiLSTM, as the inter-symbol correlations in residual nonlinearities are shorter than those in linear effects. The shorter input window reduces model scale and the number of time steps within BiLSTM, avoiding performance degradation caused by handling long-term memory. As the number of channels and symbol rate further increase, the inter-symbol correlation caused by ISI can affect thousands of symbols, making it very challenging for DL models to learn linear effects. FDD-BiLSTM incorporates a physical knowledge to model linear effects, effectively addressing this issue and offering promising application potential in wideband systems.

C. Extending FDD-BiLSTM to wideband WDM systems

FDD-BiLSTM has demonstrated excellent modeling capabilities and outperforms the other four DL approaches.

However, obvious accuracy degradation is observed in WDM configurations with more channels and higher rates. To better analyze its effectiveness in wideband WDM systems, we extend FDD-BiLSTM to WDM configurations with up to 25 channels and a symbol rate of 200 GBaud.

1) **WDM configurations with increased number of channels:** To evaluate the modeling performance of FDD-BiLSTM in WDM configurations with more channels, tests are conducted across channel configurations of [5, 13, 15, 21, 25] channels, with a fixed transmission rate of 50 GBaud and a launch power of 4 dBm per channel. Results from the previously analyzed 5-channel and 13-channel configurations are included for comprehensive comparison. As the number of channels increases, signal bandwidth expands, necessitating adjustments to the input window length within FDD-BiLSTM. Based on formulas (8) and (9), the input window lengths are adjusted to [45, 117, 135, 187, 223] symbols to account for varying nonlinear inter-symbol correlations.

The NMSE performance of FDD-BiLSTM across various channel configurations over an 800 km transmission is shown in Fig. 10(a). After 800 km transmission, the NMSE is just 3.8E-3 for the 5-channel configuration, compared to 4.49E-2 for 21-channel and 5.43E-2 for 25-channel configurations–

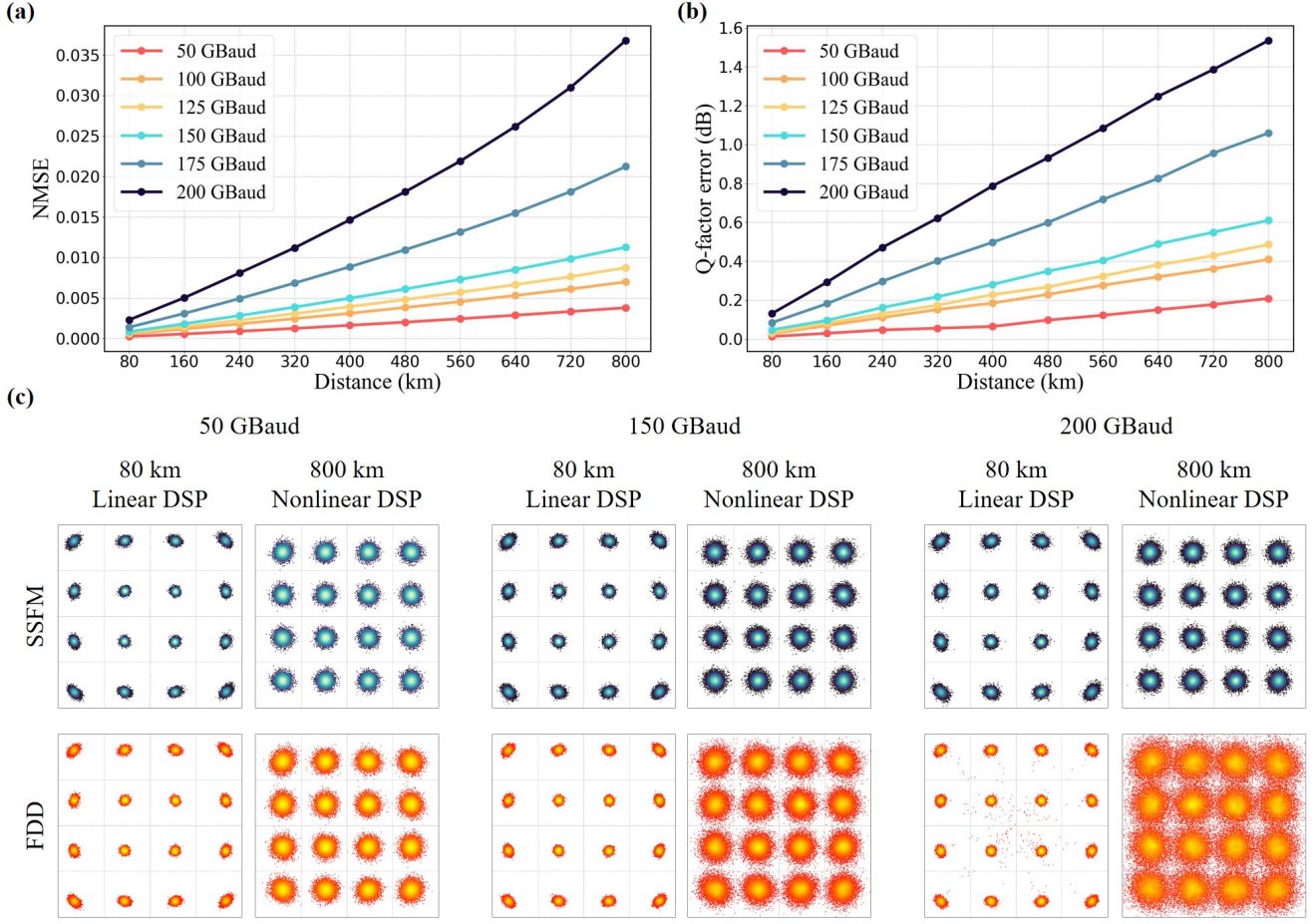


Fig. 11. The results of FDD-BiLSTM applied in higher-rate WDM systems. (a) NMSE curve of different transmission rates covering 800 km transmission. (b) Q-factor error curve after nonlinear DSP processing between FDD-BiLSTM and SSFM of different transmission rates covering 800 km transmission.

approximately an order of magnitude higher than the 5-channel case. This indicates a gradual decline in waveform modeling capacity as the number of channels increases. Further analysis of transmission performance errors is conducted using constellations and Q-factor. The first row of Fig. 10(c) shows constellations after 80 km transmission with linear DSP. The nonlinear phase rotation is clearly demonstrated in the constellations for the 5-channel and 15-channel configurations, indicating better nonlinear modeling capacity of FDD-BiLSTM. However, in the 25-channel configuration, the constellations exhibit Gaussian-like distributions, neglecting the nonlinear characteristics, which indicates a severe decline in nonlinear modeling accuracy of FDD-BiLSTM. The second row of Fig. 10(c) illustrates constellations after 800 km transmission with nonlinear DSP. Additional nonlinear impairments introduced by the multi-channel DBP algorithm become increasingly apparent with a growing number of channels, indicating more underfitting of nonlinear effects. As shown in Fig. 10(b), Q-factor errors after nonlinear DSP between SSFM and FDD-BiLSTM increase with the number of channels. For the 5-channel scenario, the Q-factor error is just 0.21 dB after 800 km transmission, compared to 2.23 dB in the 25-channel configuration—a tenfold increase, indicating a significant transmission performance gap in more-channel

configurations. The longer inter-symbol correlations, more intricate nonlinear representations, and higher sampling rate of SSFM are the main reasons for this performance degradation.

2) WDM configurations with increased symbol rates:

To evaluate the modeling performance of FDD-BiLSTM in higher-rate WDM configurations, tests are conducted using symbol rate configurations of [50, 100, 125, 150, 175, 200] Gbaud, with the number of channels fixed at 5. The optimal launch power is increased for higher symbol rates. The launch power for testing is adjusted to be approximately 2.5 dB higher than the optimized launch power, as detailed in the Table VI. As the symbol rate and spectral width increase simultaneously, the nonlinear inter-symbols correlations grow exponentially according to formulas (8) and (9). Therefore, the input window length is adjusted to [45, 163, 251, 357, 499, 651] symbols to adapt to these changes.

The NMSE performance of FDD-BiLSTM across various symbol rate configurations over an 800 km transmission is shown in Fig. 11(a). After 800 km transmission, the NMSE increases with symbol rates, which is just 3.8E-3 for 50 Gbaud configuration, compared to 2.12E-2 for 175 Gbaud and 3.68E-2 for 200 Gbaud configurations, indicating significant waveform errors in higher-rate scenarios. Further analysis of transmission performance errors is conducted using constel-

lations and Q-factor. Fig. 11(c) shows constellations after 80 km transmission with linear DSP and 800 km transmission with nonlinear DSP. The first row of each configuration shows that the trend of nonlinear phase rotation of FDD-BiLSTM compared to SSFM gradually deviates as the symbol rates increase. The second row of each configuration shows additional nonlinear impairments introduced by the multi-channel DBP algorithm, which become increasingly apparent with higher symbol rates. These results from constellations demonstrate weaker nonlinear modeling capacity of FDD-BiLSTM in higher-rate configurations. As shown in Fig. 11(b), Q-factor errors after nonlinear DSP between SSFM and FDD-BiLSTM increase with the symbol rate. For the 50 GBaud scenario, the Q-factor error is 0.21 dB after 800 km transmission, compared to 1.53 dB in the 200 GBaud configuration, indicating a more significant performance gap in higher-rate configurations. The longer inter-symbol correlations and more intricate nonlinear representations due to higher launch power are the main reasons for this performance degradation.

D. Analysis of challenges for the application of DL schemes in wideband WDM systems

The results from NMSE, constellations, and Q-factor errors collectively reveal accuracy degradation for FDD-BiLSTM as the number of channels and symbol rates increase. Here, we analyze the reasons of this accuracy degradation from three perspectives: the more intricate linear effects and nonlinear effects, as well as the higher sampling rate of the SSFM in the digital simulation system.

Linear effects, primarily CD, lead to ISI. The number of symbols affected by ISI is determined by the spectrum width and symbol rate of the WDM signals, as described by equation (7). At a fixed symbol rate, an increased number of channels widens the spectrum, thereby extending the length of ISI. Similarly, for a fixed number of channels, a higher symbol rate increases both the symbol rate and spectral width simultaneously, resulting in a quadratic growth of ISI. Moreover, nonlinear effects and linear effects occur simultaneously in optical fibers, ISI also induces inter-symbol correlations in the nonlinearities. The length of the nonlinear inter-symbol correlations is typically shorter than that caused by linear effects, as described by equations (8) and (9). To accurately capture these inter-symbol correlations, DL models must adjust their input window according to the length of ISI. For DL models without linear decoupling, the input window length must be long enough to accommodate the full length of ISI in order to accurately model linear effects. In contrast, FDD allows for shorter input windows, focusing more on capturing nonlinearities. Even in low-rate and few-channel scenarios, DL models without linear decoupling still require longer input sequences, which diminishes their accuracy, particularly in fully connected networks that handle long, one-dimensional input sequences. Temporal models, such as BiLSTM and multi-head attention, somewhat mitigate this issue due to their enhanced temporal feature extraction capabilities through recurrent structures or self-attention mechanisms. However, they still face performance degradation as the number of channels

and symbol rates increases due to the challenge of capturing long-term memory. In contrast, FDD-BiLSTM only processes shorter input sequences to model nonlinear correlations, resulting in superior performance in simpler configurations. Nevertheless, as the number of channels and symbol rates increases, accuracy degradation remains inevitable because nonlinear inter-symbol correlations continue to grow. Thus, the inter-symbol correlations induced by CD pose a significant challenge for waveform modeling in wideband WDM systems.

Nonlinear effects, primarily referring to Kerr nonlinearity, can be categorized into intra-channel and inter-channel nonlinearities. In the case of nonlinearity only, NLSE can be simplified as follows.

$$\begin{aligned} \frac{\partial E_k}{\partial z} = & -j\gamma_k \left(|E_k|^2 E_k + 2 \sum_{m \neq k} |E_m|^2 E_k \right. \\ & \left. + \sum_{n,l,m \in \mathcal{H}} E_n(z,t) E_l(z,t) E_m^*(z,t) e^{j\Delta\beta_{jlm} z} \right), \end{aligned} \quad (18)$$

where the first term on the right-hand side represents intra-channel nonlinearity, known as SPM, while the second and third terms correspond to inter-channel nonlinearities, including XPM and FWM. The overall strength of nonlinear effects is influenced by the signal power. The inter-channel nonlinearities also become more pronounced as the number of channel increases. Consequently, as the number of channels grows, inter-channel nonlinear effects increase significantly, complicating the ability of a single DL model to accurately capture these nonlinearities across all channels. Moreover, as the symbol rate increases, the optimal launch power also rises, as illustrated in Fig. 8, which further challenges the DL model by introducing stronger nonlinear effects due to higher launch powers. Therefore, the escalation of nonlinear effects, particularly the growing complexity of inter-channel nonlinearities, presents a key challenge for waveform modeling in wideband WDM systems. To address these challenges, DL models must possess enhanced nonlinear fitting capabilities to effectively model the stronger and more intricate nonlinearities encountered in these systems.

The sampling rate of SSFM in the digital simulation system is set to 4 times the number of channels, aiming to construct an analog-like signal that preserves characteristics similar to those of analog optical signals propagating through the real optical fiber channel. This scaling of the sampling rate with the number of channels is designed to prevent spectral aliasing in the full-field WDM signal, while balancing the accuracy and complexity of the SSFM algorithm. In configurations with more channels, the increased sampling rate results in each symbol containing more sampling points, which expands the input dimension and parameter scale of the DL model. While larger-scale models have the potential for better performance, they are more challenging to train to optimal levels, requiring larger datasets, extended training times, and more advanced training techniques.

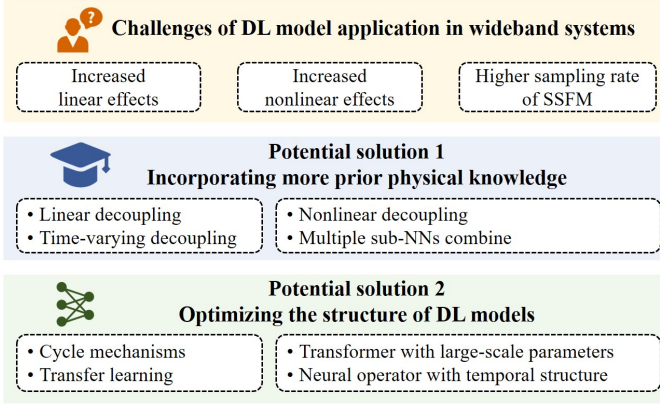


Fig. 12. Challenges and potential solutions of DL model application in wideband systems.

VI. POTENTIAL SOLUTIONS FOR ENHANCING THE ACCURACY OF DL MODELS

The performance of DL-based optical fiber channel modeling deteriorates in configurations with more-channel and higher-rate, posing significant challenges for their application in next-generation wideband optical fiber transmission systems. To address these challenges and enhance their capacity, we propose two potential strategies from the perspectives of incorporating more prior physical knowledge and optimizing the structure of DL models.

A. Incorporating more prior physical knowledge

1) Two approaches for incorporating prior physical knowledge: The comparison results in this paper demonstrate that FDD-BiLSTM, employing a distributed architecture combined with a physics-data hybrid-driven approach, outperforms purely data-driven models, particularly in multi-channel and high-rate scenarios. These results suggest that incorporating physical prior knowledge have better application prospects. FDD achieves incorporating physical knowledge by decoupling linear effects during the data preprocessing stage. Beyond this approach, another effective strategy is embedding physical constraints into the loss function, as exemplified by PINO [38]. By integrating the NLSE directly into the loss function, training can proceed in an unsupervised manner, with the input-output mapping constrained to follow the physical characteristics described by the NLSE. PINO also reduces data requirements and improves training efficiency. Despite their different methods of integration, both FDD and PINO reflect similar underlying physical mechanisms and yield comparable outcomes. In [80], the training behavior of FDD-BiLSTM and BiLSTM was analyzed through the evolution of NLSE loss. As illustrated in Fig. 13, FDD-BiLSTM shows a rapid decline in NLSE loss at the early training stages, while BiLSTM converges more slowly. This suggests that models incorporating linear decoupling can inherently learn the NLSE constraint between input and output data, even without explicitly including NLSE loss during training. These observations indicate that both methods—embedding physical prior knowledge through data preprocessing or via the loss

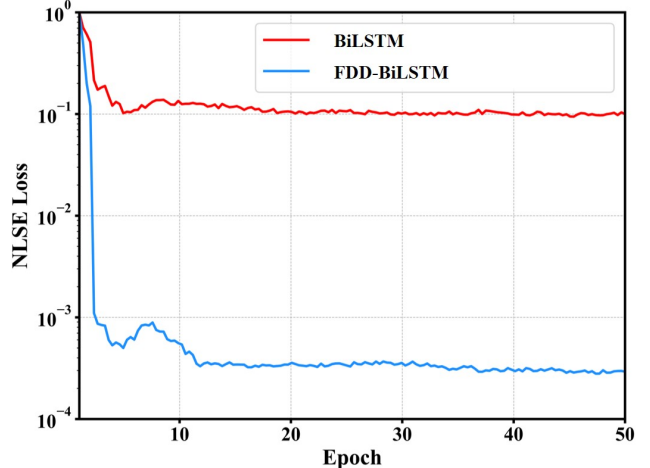


Fig. 13. The trend of NLSE loss of BiLSTM and FDD-BiLSTM during training.

function—achieve similar beneficial effects. However, despite these advances, physics-data hybrid-driven methods still suffer from significant accuracy degradation in wideband scenarios. To overcome this limitation, future schemes must incorporate richer physical knowledge by decoupling additional features—not only linear CD but also nonlinear characteristics and time-varying linear impairments — to further enhance model accuracy and robustness in complex wideband systems.

2) Nonlinear characteristic decoupling: As discussed in Section V, the enhanced nonlinear effects in wideband WDM systems significantly limit the performance of DL models, particularly due to the more intricate inter-channel nonlinear effects introduced by an increased number of channels. Decoupling these nonlinear effects offers a promising solution to address this challenge. Current DL schemes typically employ a single model to handle all nonlinearities across multiple channels, which limits the model's ability to effectively capture these complex interactions. A potential solution, based on the characterization of the nonlinear term in the NLSE, is to tackle different nonlinear effects separately. In [43], stacked DeepONet structures have been employed for optical fiber channel waveform modeling in WDM systems covering the C + L band. This approach employs multiple DeepONets, each designed to fit the intra-channel nonlinearities of individual WDM channels. By isolating the nonlinearities within each channel, this method simplifies the complexity for each DeepONet, enabling more efficient modeling of multi-channel signals. While this method does not directly address inter-channel nonlinearities, it offers a promising direction for future model development. In [81], a strategy involving multiple sub-neural networks was applied to nonlinearity compensation. These sub-networks separately handle intra-channel and inter-channel nonlinearities across various subcarriers, improving accuracy by reducing the learning complexity for each individual network. These results suggest that decoupling nonlinearities and using distinct sub-networks to separately address intra-channel and inter-channel effects can significantly enhance modeling accuracy in wideband WDM systems.

3) **Time-varying linear characteristic decoupling:** Existing DL models are typically employed as replacements for SSFM, focusing primarily on the static linear and nonlinear effects of optical fibers, while overlooking dynamic linear impairments such as state of polarization (SOP) fluctuations, polarization mode dispersion (PMD), phase noise (PN), and frequency offset (FO) introduced by the laser. To more accurately reflect real-world optical transmission systems, these dynamic effects must be incorporated. However, DL models are inherently more adept at capturing deterministic system responses and struggle with modeling dynamic, time-varying behaviors. In contrast, advanced DSP algorithms grounded in physical models—including multiple-input multiple-output (MIMO) equalizers, frequency offset estimation (FOE), and carrier phase recovery (CPR)—excel in compensating for dynamic linear impairments. These algorithms offer a pathway to separate dynamic linear effects from the transmitted signal, enabling the creation of datasets that isolate deterministic nonlinear effects for more effective DL model training. A digital twin (DT) framework proposed in [82] integrates these DSP algorithms with DL models to mirror real optical fiber transmission systems. In this framework, dynamic linear effects are decoupled by DSP modules, producing labels that preserve only residual deterministic effects for neural network training. The demonstrated success of this DT framework provides a promising solution for addressing dynamic linear effects, paving the way for more realistic DL-based optical channel modeling.

B. Optimizing the structure of DL models

In addition to incorporating more physical prior knowledge, optimizing a DL model structure that conforms to the characteristics of fiber channel is also a potential solution to address the challenges such as longer inter-symbol correlations and stronger nonlinear effects.

1) **Enhancing the capacity for addressing longer inter-symbol correlations:** To effectively capture longer inter-symbol correlations, DL models require input sequences enriched with more adjacent symbols, enabling accurate prediction of the current output symbol. However, this results in significantly longer input sequences, increasing model scale, computational complexity, and training difficulty. One promising solution to mitigate these challenges is to reuse computational results from adjacent symbols, reducing repeated calculations. The Co-LSTM architecture introduces a recycling mechanism during inference, reusing outputs from adjacent LSTM cells to lower computational repetition and simplify the complexity of conventional LSTM structures. This approach has demonstrated both high accuracy and reduced complexity in waveform modeling [37] and nonlinear compensation [83] tasks. Beyond inference optimization, improving training efficiency for large-scale models with more time steps during limited datasets and constrained training resources is equally critical. Transfer learning [84] emerges as an effective strategy, leveraging multi-stage training to address these issues. Its feasibility in waveform modeling can be justified from two perspectives: the characteristics of optical fiber channels and

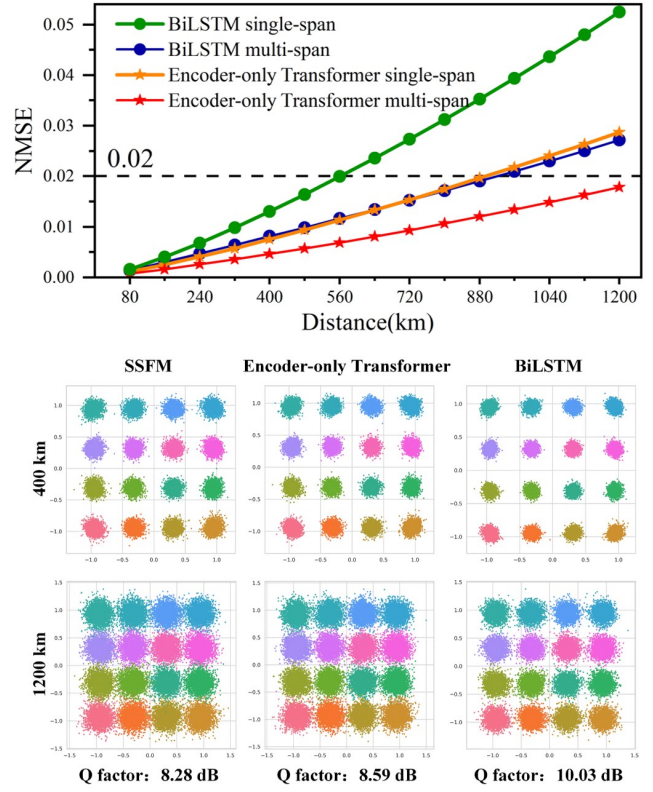


Fig. 14. The results of Encoder-only Transformer and BiLSTM integrated with FDD.

the structures of temporal DL models. From the perspective of channel characteristics, nonlinear inter-symbol correlations are predominantly influenced by the closest adjacent symbols, while the influence of distant symbols is relatively weaker [85]. This allows DL models to initially focus on learning the dominant nonlinear effects from nearby symbols and subsequently extend to capture weaker influence from distant symbols via transfer learning. From the perspective of DL model structure, temporal neural networks such as BiLSTM and multi-head attention mechanisms divide the input sequence across different time steps. BiLSTM employs recurrent units with shared parameters to process each time step, while the multi-head attention mechanism captures inter-symbol correlations through the cross-correlation among Query (Q), Key (K), Value (V) matrices [86], with linear transformations of Q, K, V perform in parallel. These designs enable both BiLSTM and multi-head attention to expand the length of the input sequence by increasing additional number of calculations for time units rather than adding new model parameters. Therefore, based on the nonlinear channel characteristics and model structures, a small-scale model with shorter input sequences can be trained to learn dominant inter-symbol correlations from the closest adjacent symbols. This model can then be fine-tuned into a large-scale version with longer input sequences to capture residual nonlinearities from distant symbols, using transfer learning while maintaining the same parameter scale. The small-scale model benefits from faster convergence on limited data, and the large-scale model fine-tuned from it achieves im-

proved convergence speed and higher final accuracy. This two-stage transfer learning approach offers a promising solution to the challenges posed by long-term correlations, balancing accuracy and computational complexity.

2) *Enhancing the capacity for fitting stronger nonlinear effects*: To enhance the nonlinear fitting capacity of DL models and address the challenge of modeling stronger nonlinear effects, increasing the number of model parameters is a direct and effective strategy. Meanwhile, it is essential to design architectures that can efficiently accommodate large parameter counts. Prior studies [87] have demonstrated a correlation between model scale and accuracy, indicating that larger models tend to deliver better performance. However, for architectures such as LSTM, simply scaling up parameters often leads to diminishing returns due to inherent bottlenecks in model capacity [88]. In contrast, the Transformer architecture, with its multi-head attention mechanism, has demonstrated exceptional scalability, supporting models with tens of billions of parameters, as exemplified by large language models (LLMs) [89]–[91]. Within this large-scale parameter range, a consistent positive relationship between parameter count and performance has been observed, with emergent capabilities appearing beyond critical thresholds [87]. Thus, designing DL models based on multi-head attention mechanisms offers a promising path for scaling parameters and handling increasingly complex nonlinear modeling tasks. For instance, an Encoder-only Transformer [42], integrated with FDD, has been shown to outperform BiLSTM for optical channel modeling in a 21-channel WDM system, as illustrated in Fig. 14. Beyond conventional neural networks, neural operators have emerged as a compelling approach due to their strong generalization capabilities. Although, current comparisons indicate that models like DeepONet and FNO have yet to deliver outstanding performance for wideband WDM systems. Their primary limitation lies in their fully connected architectures, which are less suitable for scenarios requiring extended input windows to capture long ISI. A promising direction involves embedding temporal architectures within neural operator frameworks. For example, DeepONet's flexible trunk and branch network structures could be enhanced by replacing fully connected layers with temporal architectures, enabling them to better capture long inter-symbol correlations and address the challenges posed by stronger nonlinearities and extended ISI in wideband systems.

VII. CONCLUSION

In this paper, we review the DL-based optical fiber channel waveform modeling schemes and elaborate on their respective characteristics, inducing overall and distributed schemes, pure data-driven and physics-data hybrid driven schemes, neural networks and neural operators. To assess and compare their performance in WDM systems, we propose a DSP-assisted accuracy evaluation method that addresses the limitations of traditional accuracy metrics, such as the difficulty in defining an acceptable NMSE threshold and the inconsistency between waveform errors and transmission performance errors. This method, integrated with nonlinear DSP algorithms,

ensures alignment between waveform errors and transmission performance errors, providing a fair benchmark for evaluating the accuracy of DL models.

Using this method, we conduct a comprehensive comparison of DL schemes across scenarios ranging from few-channel, low-rate to wideband configurations. In a 5-channel, 50 GBaud scenario, distributed schemes outperform overall schemes. Among distributed schemes, temporal neural networks, such as BiLSTM, multi-head attention, and FDD-BiLSTM, surpass fully connected networks like FNO and DeepONet, demonstrating an 83.1% improvement in NMSE and a 1.06 dB reduction in Q-factor error. As we extend the tests to more channels and higher rates, including a 13-channel, 50 GBaud configuration and a 5-channel, 100 GBaud setup, the performance advantages of FDD-BiLSTM improves further due to its incorporation of physical knowledge. However, as the number of channels and symbol rates increase, the performance of FDD still gradually deteriorate: NMSE increases by 92.9%, and Q-factor errors rise by 2.02 dB when scaling from 5 to 25 channels; similarly, NMSE degrades by 89.7%, and Q-factor errors increase by 1.33 dB when symbol rates increase from 50 to 200 GBaud.

We analyze the challenges involved in scaling DL models to wideband configurations, including the more intricate linear and nonlinear effects, as well as the higher sampling rates of SSFM. Finally, we discuss potential solutions to address these challenges and enhance the applicability of DL schemes in wideband systems, such as incorporating more prior physical knowledge and optimizing the structure of DL models. With ongoing technological advancements, we believe these challenges will be gradually overcome, positioning DL schemes as a promising waveform modeling technology for the next-generation optical network.

ACKNOWLEDGMENTS

The authors acknowledge the funding provided by the National Key R&D Program of China (2023YFB2905400), National Natural Science Foundation of China (62025503), and Shanghai Jiao Tong University 2030 Initiative.

REFERENCES

- [1] A. Ferrari *et al.*, “Assessment on the achievable throughput of multi-band ITU-T G.652.D fiber transmission systems,” *J. Lightw. Technol.*, vol. 38, no. 16, pp. 4279–4291, 2020.
- [2] M. Zuo *et al.*, “Field trial of real-time $80\text{-}\lambda\times400\text{-Gb/s}$ single-carrier 128-GBd DP-QPSK transmission covering 12-THz C+L band over 2502-km terrestrial G.652.D fibre,” in *49th European Conference on Optical Communications (ECOC 2023)*, vol. 2023, 2023, pp. 843–846.
- [3] D. Ge *et al.*, “Fully-loaded $80\times400\text{Gb/s}$ DP-QPSK transmission with commercial 12-THz C6T+L6T EDFA over record distance of 7000km,” in *2023 Asia Communications and Photonics Conference/2023 International Photonics and Optoelectronics Meetings (ACP/POEM)*, 2023, pp. 1–4.
- [4] S. Escobar-Landero, A. Lorences-Riesgo, X. Zhao, Y. Frignac, and G. Charlet, “S+C+L high-capacity transmission systems: Challenges and opportunities,” *J. Lightw. Technol.*, vol. 42, no. 12, pp. 4260–4270, 2024.
- [5] Y. Frignac *et al.*, “Record 158.4 Tb/s transmission over 2x60 km field SMF using S+C+L 18Thz-bandwidth lumped amplification,” in *49th European Conference on Optical Communications (ECOC 2023)*, vol. 2023, 2023, pp. 550–553.
- [6] Y. Zhang *et al.*, “Optical power control for GSNR optimization based on C+L-band digital twin systems,” *J. Lightw. Technol.*, vol. 42, no. 1, pp. 95–105, Jan 2024.

[7] B. Correia, R. Sadeghi, E. Virgillito, A. Napoli, N. Costa, J. Pedro, and V. Curri, "Optical power control strategies for optimized C+L+S-bands network performance," in *2021 Optical Fiber Communications Conference and Exhibition (OFC)*, 2021, pp. 1–3.

[8] I. Roberts, J. M. Kahn, J. Harley, and D. W. Boertjes, "Channel power optimization of WDM systems following gaussian noise nonlinearity model in presence of stimulated raman scattering," *J. Lightw. Technol.*, vol. 35, no. 23, pp. 5237–5249, 2017.

[9] Y. Song, Q. Fan, C. Lu, D. Wang, and A. P. T. Lau, "Efficient three-step amplifier configuration algorithm for dynamic C+L-band links in presence of stimulated raman scattering," *J. Lightw. Technol.*, vol. 41, no. 5, pp. 1445–1453, 2023.

[10] C. Zhang *et al.*, "Potential failure cause identification for optical networks using deep learning with an attention mechanism," *IEEE J. Opt. Commun. Netw.*, vol. 14, no. 2, pp. A122–A133, 2022.

[11] Y. Zhang *et al.*, "Building a digital twin for large-scale and dynamic C+L-band optical networks," *IEEE J. Opt. Commun. Netw.*, vol. 15, no. 12, pp. 985–998, 2023.

[12] A. Napoli *et al.*, "Reduced complexity digital back-propagation methods for optical communication systems," *J. Lightw. Technol.*, vol. 32, no. 7, pp. 1351–1362, 2014.

[13] O. Vassilieva, I. Kim, and T. Ikeuchi, "Enabling technologies for fiber nonlinearity mitigation in high capacity transmission systems," *J. Lightw. Technol.*, vol. 37, no. 1, pp. 50–60, 2019.

[14] Q. Fan, G. Zhou, T. Gui, C. Lu, and A. P. T. Lau, "Advancing theoretical understanding and practical performance of signal processing for nonlinear optical communications through machine learning," *Nat. Commun.*, vol. 11, p. 3694, 07 2020.

[15] O. Sidelnikov, A. Redyuk, S. Sygletos, M. Fedoruk, and S. Turitsyn, "Advanced convolutional neural networks for nonlinearity mitigation in long-haul WDM transmission systems," *J. Lightw. Technol.*, vol. 39, no. 8, pp. 2397–2406, 2021.

[16] X. Lin, S. Luo, S. K. O. Soman, O. A. Dobre, L. Lampe, D. Chang, and C. Li, "Perturbation theory-aided learned digital back-propagation scheme for optical fiber nonlinearity compensation," *J. Lightw. Technol.*, vol. 40, no. 7, pp. 1981–1988, 2022.

[17] Z. Niu, H. Yang, L. Li, M. Shi, G. Xu, W. Hu, and L. Yi, "Learnable digital signal processing: a new benchmark of linearity compensation for optical fiber communications," *Light Sci. Appl.*, vol. 13, no. 1, p. 188, 2024.

[18] B. Karanov *et al.*, "End-to-end deep learning of optical fiber communications," *J. Lightw. Technol.*, vol. 36, no. 20, pp. 4843–4855, 2018.

[19] B. Karanov, D. Lavery, P. Bayvel, and L. Schmalen, "End-to-end optimized transmission over dispersive intensity-modulated channels using bidirectional recurrent neural networks," *Opt. Express*, vol. 27, no. 14, pp. 19 650–19 663, Jul 2019.

[20] B. Karanov, M. Chagnon, V. Aref, D. Lavery, P. Bayvel, and L. Schmalen, "Optical fiber communication systems based on end-to-end deep learning : (invited paper)," in *2020 IEEE Photonics Conference (IPC)*, 2020, pp. 1–2.

[21] Z. Niu, H. Yang, H. Zhao, C. Dai, W. Hu, and L. Yi, "End-to-end deep learning for long-haul fiber transmission using differentiable surrogate channel," *J. Lightw. Technol.*, vol. 40, no. 9, pp. 2807–2822, 2022.

[22] Y. Xu, L. Huang, W. Jiang, X. Guan, W. Hu, and L. Yi, "End-to-end learning for 100G-PON based on noise adaptation network," *J. Lightw. Technol.*, vol. 42, no. 7, pp. 2328–2337, 2024.

[23] M. Li and S. Wang, "End-to-end learning for chromatic dispersion compensation in optical fiber communication," *IEEE Commun. Lett.*, vol. 26, no. 8, pp. 1829–1832, 2022.

[24] J. Song, C. Häger, J. Schröder, A. G. I. Amat, and H. Wymeersch, "Model-based End-to-End learning for WDM systems with transceiver hardware impairments," *IEEE J. Sel. Top. Quantum Electron.*, vol. 28, no. 4: Mach. Learn. in Photon. Commun. and Meas. Syst., pp. 1–14, 2022.

[25] D. Glogé, "Optical fibers for communication," *Appl. Opt.*, vol. 13, no. 2, pp. 249–254, Feb 1974.

[26] P. Poggiolini, "The GN model of non-linear propagation in uncompensated coherent optical systems," *J. Lightw. Technol.*, vol. 30, no. 24, pp. 3857–3879, 2012.

[27] A. Carena, G. Bosco, V. Curri, Y. Jiang, P. Poggiolini, and F. Forghieri, "EGN model of non-linear fiber propagation," *Opt. Express*, vol. 22, no. 13, pp. 16 335–16 362, Jun 2014.

[28] G. P. Agrawal, "Nonlinear fiber optics," in *Nonlinear Science at the Dawn of the 21st Century*, P. L. Christiansen, M. P. Sørensen, and A. C. Scott, Eds. Berlin, Heidelberg: Springer Berlin Heidelberg, 2000, pp. 195–211.

[29] P. Serena, C. Lasagni, S. Musetti, and A. Bononi, "On numerical simulations of ultra-wideband long-haul optical communication systems," *J. Lightw. Technol.*, vol. 38, no. 5, pp. 1019–1031, 2020.

[30] K. Hornik, M. Stinchcombe, and H. White, "Multilayer feedforward networks are universal approximators," *Neural Networks*, vol. 2, no. 5, pp. 359–366, 1989.

[31] J. Wei, X. Zhang, Z. Ji *et al.*, "Deploying and scaling distributed parallel deep neural networks on the tianhe-3 prototype system," *Sci. Rep.*, vol. 11, p. 20244, 2021.

[32] D. Wang *et al.*, "Data-driven optical fiber channel modeling: A deep learning approach," *J. Lightw. Technol.*, vol. 38, no. 17, pp. 4730–4743, 2020.

[33] H. Yang, Z. Niu, S. Xiao, J. Fang, Z. Liu, D. Fainsin, and L. Yi, "Fast and accurate optical fiber channel modeling using generative adversarial network," *J. Lightw. Technol.*, vol. 39, no. 5, pp. 1322–1333, 2021.

[34] Y. Zang, Z. Yu, K. Xu, M. Chen, S. Yang, and H. Chen, "Multi-span long-haul fiber transmission model based on cascaded neural networks with multi-head attention mechanism," *J. Lightw. Technol.*, vol. 40, no. 19, pp. 6347–6358, 2022.

[35] ———, "Data-driven fiber model based on the deep neural network with multi-head attention mechanism," *Opt. Express*, vol. 30, no. 26, pp. 46 626–46 648, Dec 2022.

[36] X. He *et al.*, "Fourier neural operator for accurate optical fiber modeling with low complexity," *J. Lightw. Technol.*, vol. 41, no. 8, pp. 2301–2311, 2023.

[37] J. Zheng, T. Zhang, and F. Zhang, "Co-lstm-based fiber link modeling with ase noise tracking for long-haul coherent optical transmission," *Opt. Lett.*, vol. 49, no. 7, pp. 1848–1851, Apr 2024.

[38] Y. Song, D. Wang, Q. Fan, X. Jiang, X. Luo, and M. Zhang, "Physics-informed neural operator for fast and scalable optical fiber channel modelling in multi-span transmission," in *2022 European Conference on Optical Communication (ECOC)*, 2022, pp. 1–4.

[39] R. Jiang, Z. Fu, Y. Bao, H. Wang, X. Ding, and Z. Wang, "Data-driven method for nonlinear optical fiber channel modeling based on deep neural network," *IEEE Photon. J.*, vol. 14, no. 4, pp. 1–8, 2022.

[40] Q. Qiu, H. Lun, X. Liu, L. Yi, W. Hu, and Q. Zhuge, "Fourier neural operator based fibre channel modelling for optical transmission," in *2022 European Conference on Optical Communication (ECOC)*, 2022, pp. 1–4.

[41] H. Yang, Z. Niu, H. Zhao, S. Xiao, W. Hu, and L. Yi, "Fast and accurate waveform modeling of long-haul multi-channel optical fiber transmission using a hybrid model-data driven scheme," *J. Lightw. Technol.*, vol. 40, no. 14, pp. 4571–4580, 2022.

[42] M. Shi, H. Yang, Z. Niu, C. Zeng, S. Xiao, W. Hu, and L. Yi, "Accurate and efficient optical fiber WDM transmission modeling using the encoder-only transformer with feature decoupling distributed method," in *2023 Asia Communications and Photonics Conference/2023 International Photonics and Optoelectronics Meetings (ACP/POEM)*, 2023, pp. 1–5.

[43] X. Zhang, M. Zhang, Y. Song, X. Jiang, F. Zhang, and D. Wang, "Deeponet-based waveform-level simulation for a wideband nonlinear WDM system," *J. Lightw. Technol.*, vol. 41, no. 22, pp. 6908–6922, 2023.

[44] G. Ye, J. Xiang, G. Zhou, M. Xiang, J. Li, Y. Qin, and S. Fu, "Impact of the input OSNR on data-driven optical fiber channel modeling," *IEEE J. Opt. Commun. Netw.*, vol. 15, no. 2, pp. 78–86, 2023.

[45] C. Zeng, Z. Niu, H. Yang, M. Shi, W. Hu, and L. Yi, "Enhancing generalization in neural channel model for optical fiber WDM transmission through learned encoding of system parameters," in *2024 Optical Fiber Communications Conference and Exhibition (OFC)*, 2024, pp. 1–3.

[46] R. Jiang, Z. Wang, T. Jia, Z. Fu, C. Shang, and C. Wu, "Flexible optical fiber channel modeling based on a neural network module," *Opt. Lett.*, vol. 48, no. 16, pp. 4332–4335, Aug 2023.

[47] M. Ma, H. Chang, R. Gao, D. Guo, X. Liu, and M. Yuan, "Modeling of multi-core fiber channel based on m-cgan for high capacity fiber optical communication," in *2023 Asia Communications and Photonics Conference/2023 International Photonics and Optoelectronics Meetings (ACP/POEM)*, 2023, pp. 01–05.

[48] M. Yuan *et al.*, "A conditional generative adversarial network aided few-mode fiber channel modeling for large-capacity optical fiber communication," in *2023 21st International Conference on Optical Communications and Networks (ICOON)*, 2023, pp. 1–3.

[49] Y. Zhu, J. Ye, L. Yan, T. Zhou, P. Li, X. Zou, and W. Pan, "Transformer-based high-fidelity modeling method for radio over fiber link," *J. Lightw. Technol.*, vol. 41, no. 9, pp. 2657–2665, 2023.

[50] N. Zhang, H. Yang, Z. Niu, L. Zheng, C. Chen, S. Xiao, and L. Yi, "Transformer-based long distance fiber channel modeling for optical

OFDM systems,” *J. Lightw. Technol.*, vol. 40, no. 24, pp. 7779–7789, 2022.

[51] W. Chen *et al.*, “Deep learning-based channel modeling for free space optical communications,” *J. Lightw. Technol.*, vol. 41, no. 1, pp. 183–198, 2023.

[52] S. Boscolo and C. Finot, “Artificial neural networks for nonlinear pulse shaping in optical fibers,” *Opt. Laser Technol.*, vol. 131, p. 106439, 2020.

[53] T. Zahavy, A. Dikopoltsev, D. Moss, G. I. Haham, O. Cohen, S. Mannor, and M. Segev, “Deep learning reconstruction of ultrashort pulses,” *Optica*, vol. 5, no. 5, pp. 666–673, 2018.

[54] L. Salmela, N. Tspinakis, A. Foi, C. Bille, J. M. Dudley, and G. Genty, “Predicting ultrafast nonlinear dynamics in fibre optics with a recurrent neural network,” *Nat. Mach. Intell.*, vol. 3, no. 4, pp. 344–354, 2021.

[55] H. Yang, H. Zhao, Z. Niu, G. Pu, S. Xiao, W. Hu, and L. Yi, “Low-complexity full-field ultrafast nonlinear dynamics prediction by a convolutional feature separation modeling method,” *Opt. Express*, vol. 30, no. 24, pp. 43 691–43 705, 2022.

[56] U. Teğin, B. Rahmani, E. Kakkava, N. Borhani, C. Moser, and D. Psaltis, “Controlling spatiotemporal nonlinearities in multimode fibers with deep neural networks,” *Appl. Photonics*, vol. 5, no. 3, 2020.

[57] M. Raissi, P. Perdikaris, and G. E. Karniadakis, “Physics-informed neural networks: A deep learning framework for solving forward and inverse problems involving nonlinear partial differential equations,” *J. Comput. Phys.*, vol. 378, pp. 686–707, 2019.

[58] X.-M. Liu, Z.-Y. Zhang, and W.-J. Liu, “Physics-informed neural network method for predicting soliton dynamics supported by complex parity-time symmetric potentials,” *Chin. Phys. Lett.*, vol. 40, no. 7, p. 070501, 2023.

[59] S.-Y. Xu, Q. Zhou, and W. Liu, “Prediction of soliton evolution and equation parameters for nls–mb equation based on the phipnn algorithm,” *Nonlinear Dyn.*, vol. 111, no. 19, pp. 18 401–18 417, 2023.

[60] X. Jiang, D. Wang, Q. Fan, M. Zhang, C. Lu, and A. P. T. Lau, “Solving the nonlinear schrödinger equation in optical fibers using physics-informed neural network,” in *Optical fiber communication conference*. Optica Publishing Group, 2021, pp. M3H–8.

[61] D. Wang, X. Jiang, Y. Song, M. Fu, Z. Zhang, X. Chen, and M. Zhang, “Applications of physics-informed neural network for optical fiber communications,” *IEEE Commun. Mag.*, vol. 60, no. 9, pp. 32–37, 2022.

[62] X. Jiang, D. Wang, Q. Fan, M. Zhang, C. Lu, and A. P. T. Lau, “Physics-informed neural network for nonlinear dynamics in fiber optics,” *Laser Photonics Rev.*, vol. 16, no. 9, p. 2100483, 2022.

[63] C. Menyuk, “Nonlinear pulse propagation in birefringent optical fibers,” *IEEE J. Quantum Electron.*, vol. 23, no. 2, pp. 174–176, 1987.

[64] D. Marcuse, C. Manyuk, and P. Wai, “Application of the manakov-pmd equation to studies of signal propagation in optical fibers with randomly varying birefringence,” *J. Lightw. Technol.*, vol. 15, no. 9, pp. 1735–1746, 1997.

[65] S. Evangelides, L. Mollenauer, J. Gordon, and N. Bergano, “Polarization multiplexing with solitons,” *J. Lightw. Technol.*, vol. 10, no. 1, pp. 28–35, 1992.

[66] J. Shao, X. Liang, and S. Kumar, “Comparison of split-step Fourier schemes for simulating fiber optic communication systems,” *IEEE Photon. J.*, vol. 6, no. 4, pp. 1–15, 2014.

[67] O. Sinkin, R. Holzlöhner, J. Zweck, and C. Menyuk, “Optimization of the split-step Fourier method in modeling optical-fiber communications systems,” *J. Lightw. Technol.*, vol. 21, no. 1, pp. 61–68, 2003.

[68] E. Ip and J. M. Kahn, “Compensation of dispersion and nonlinear impairments using digital backpropagation,” *J. Lightw. Technol.*, vol. 26, no. 20, pp. 3416–3425, 2008.

[69] D. Saxena, J. Cao *et al.*, “Generative adversarial networks (GANs): challenges, solutions, and future directions,” *ACM Comput. Surv.*, vol. 54, no. 3, pp. 1–42, 2022.

[70] J. Gui, Z. Sun, Y. Wen, D. Tao, and J. Ye, “A review on generative adversarial networks: Algorithms, theory, and applications,” 2020. [Online]. Available: <https://arxiv.org/abs/2001.06937>

[71] T. Chen and H. Chen, “Approximation capability to functions of several variables, nonlinear functionals, and operators by radial basis function neural networks,” *IEEE Trans. Neural Networks*, vol. 6, no. 4, pp. 904–910, 1995.

[72] S. Wang, H. Wang, and P. Perdikaris, “Learning the solution operator of parametric partial differential equations with physics-informed deep-ponets,” *Sci. Adv.*, vol. 7, no. 40, p. eabi8605, 2021.

[73] L. Lu, P. Jin, G. Pang, Z. Zhang, and G. E. Karniadakis, “Learning nonlinear operators via deeponet based on the universal approximation theorem of operators,” *Nat. Mach. Intell.*, vol. 3, no. 3, pp. 218–229, 2021.

[74] T. A. Eriksson, H. Bülow, and A. Leven, “Applying neural networks in optical communication systems: Possible pitfalls,” *IEEE Photonics Technol. Lett.*, vol. 29, no. 23, pp. 2091–2094, 2017.

[75] L. Yi, T. Liao, L. Huang, L. Xue, P. Li, and W. Hu, “Machine learning for 100 Gb/s/λ passive optical network,” *J. Lightw. Technol.*, vol. 37, no. 6, pp. 1621–1630, 2019.

[76] D. P. Kingma and J. Ba, “Adam: A method for stochastic optimization,” 2017. [Online]. Available: <https://arxiv.org/abs/1412.6980>

[77] I. Loshchilov and F. Hutter, “Sgdr: Stochastic gradient descent with warm restarts,” 2017. [Online]. Available: <https://arxiv.org/abs/1608.03983>

[78] J. Zhang, X. Li, Y. Hu, M. S. Alam, and D. V. Plant, “Spectrally efficient integrated silicon photonic phase-diverse DD receiver with near-ideal phase response for c-band DWDM transmission,” *Laser Photonics Rev.*, vol. 18, no. 3, p. 2300623, 2024.

[79] Z. Tao, L. Dou, W. Yan, L. Li, T. Hoshida, and J. C. Rasmussen, “Multiplier-free intrachannel nonlinearity compensating algorithm operating at symbol rate,” *J. Lightw. Technol.*, vol. 29, no. 17, pp. 2570–2576, 2011.

[80] Y. Zhang, Z. Niu, M. Shi, W. Hu, and L. Yi, “Improve the fitting accuracy of deep learning for the nonlinear schrödinger equation using linear feature decoupling method,” in *2024 Asia Communications and Photonics Conference (ACP) and International Conference on Information Photonics and Optical Communications (IPOC)*, 2024, pp. 1–4.

[81] A. Bakhshali, H. Najafi, B. B. Hamgini, and Z. Zhang, “Neural network architectures for optical channel nonlinear compensation in digital subcarrier multiplexing systems,” *Opt. Express*, vol. 31, no. 16, pp. 26 418–26 434, Jul 2023.

[82] H. Yang *et al.*, “The digital twin framework for the physical wideband and long-haul optical fiber communication systems,” *Laser Photonics Rev.*, vol. 18, no. 10, p. 2400234, 2024.

[83] H. Ming, X. Chen, X. Fang, L. Zhang, C. Li, and F. Zhang, “Ultralow complexity long short-term memory network for fiber nonlinearity mitigation in coherent optical communication systems,” *J. Lightw. Technol.*, vol. 40, no. 8, pp. 2427–2434, 2022.

[84] S. J. Pan and Q. Yang, “A survey on transfer learning,” *IEEE Trans. Knowl. Data Eng.*, vol. 22, no. 10, pp. 1345–1359, 2010.

[85] S. Deligiannidis, C. Mesaritakis, and A. Bogris, “Performance and complexity analysis of bi-directional recurrent neural network models versus voltaer nonlinear equalizers in digital coherent systems,” *J. Lightw. Technol.*, vol. 39, no. 18, pp. 5791–5798, 2021.

[86] A. Vaswani *et al.*, “Attention is all you need,” 2023. [Online]. Available: <https://arxiv.org/abs/1706.03762>

[87] J. Kaplan *et al.*, “Scaling laws for neural language models,” 2020. [Online]. Available: <https://arxiv.org/abs/2001.08361>

[88] S. Karita *et al.*, “A comparative study on transformer vs rnn in speech applications,” in *2019 IEEE Automatic Speech Recognition and Understanding Workshop (ASRU)*, 2019, pp. 449–456.

[89] A. Radford, K. Narasimhan, T. Salimans, I. Sutskever *et al.*, “Improving language understanding by generative pre-training,” 2018.

[90] A. Radford, J. Wu, R. Child, D. Luan, D. Amodei, I. Sutskever *et al.*, “Language models are unsupervised multitask learners,” *OpenAI blog*, vol. 1, no. 8, p. 9, 2019.

[91] T. Brown *et al.*, “Language models are few-shot learners,” *Advances in neural information processing systems*, vol. 33, pp. 1877–1901, 2020.